Heliyon 10 (2024) e37178

Contents lists available at ScienceDirect

Heliyon

journal homepage: www.cell.com/heliyon

Research article

Multi-modal neuroprotection of *Argemone mexicana* L. against Alzheimer's disease: *In vitro* and *in silico* study

Md. Enamul Kabir Talukder [a], Shahina Akhter [b], Foysal Ahammad [c], Asmim Aktar [a], Md. Saidul Islam [d], Aysha Akter Laboni [e], Mirola Afroze [e], Mala Khan [e], Mohammad Jashim Uddin [f,**], Md. Mashiar Rahman [a,*]

[a] *Molecular and Cellular Biology Laboratory, Department of Genetic Engineering and Biotechnology, Jashore University of Science and Technology, Jashore, 7408, Bangladesh*
[b] *Department of Biochemistry and Biotechnology, University of Science and Technology Chittagong (USTC), Foy's Lake, Chittagong, 4202, Bangladesh*
[c] *Laboratory of Computational Biology, Biological Solution Centre (BioSol Centre), Jashore, 7408, Bangladesh*
[d] *Korea Institute of Radiological & Medical Sciences, 75, Nowon-ro, Nowon-gu, Seoul, South Korea*
[e] *Bangladesh Reference Institute for Chemical Measurements (BRICM), Bangladesh Council of Scientific and Industrial Research, Dr Qudrat-i-Khuda Road, Dhanmondi, Dhaka, 1205, Bangladesh*
[f] *Department of Pharmacy, Jashore University of Science and Technology, Jashore, 7408, Bangladesh*

A R T I C L E I N F O

Keywords:
Argemone mexicana L.
Alzheimer's disease
Phytochemicals
Acetylcholinesterase
Butyrylcholinesterase
β-secretase
Glycogen synthase kinase-3β

A B S T R A C T

Argemone mexicana L. is a medicinal plant, but its impact on Alzheimer's disease (AD) is right now undetermined. We intended to investigate the in-vitro anti-AD potential of leaves and flowers of *A. mexicana* methanol, ethanol, and ethyl extracts and to identify multi-modal anti-AD phytochemicals by computational approaches. Molecular docking of 196 phytochemicals identified three hit phytochemicals (protoberberine, protopine, and codeine) with higher binding affinity and multi-targeting ability toward AChE, BChE, BACE-1, and GSK-3β. Further MM-GBSA assays confirmed the integrity of these phytochemicals as the hit phytochemicals. However, these phytochemicals demonstrated favorable pharmacokinetics (PK) and drugable properties having no toxicity. Molecular dynamics simulations confirmed the binding strength of the hit phytoconstituents in the active pockets of AChE, BChE, BACE-1, and GSK-3β with multi-targeting inhibitory activities. All the extracts exhibited dose-dependent antioxidant and anticholinesterase activities supporting the *insilico* results in the context of oxidative stress and cholinergic pathways. Our results offer scientific validation of the anti-AD properties of *Argemone mexicana* L. and identified protoberberine, protopine, and codeine that could be used for the development of multi-modal inhibitors of AChE, BChE, BACE-1, and GSK-3β to combat AD. Additional *in vivo* validation is recommended to ensure a thorough assessment in the present research.

* Corresponding author.
** Corresponding author.
E-mail addresses: j.uddin@just.edu.bd (M.J. Uddin), mm.rahman@just.edu.bd (Md.M. Rahman).

https://doi.org/10.1016/j.heliyon.2024.e37178
Received 16 August 2024; Accepted 28 August 2024
Available online 30 August 2024

Abbreviations

AChE	Acetylcholinesterase
BACE-1	Beta Secretase-1
BChE	Butyrylcholinesterase
FT-IR	Fourier Transform Infrared Spectroscopy
GC-MS	Gas Chromatography-Mass Spectrometry
GSK-3β	Glycogen Synthase Kinase-3 Beta
MDS	Molecular Dynamics Simulation
MolSA	Molecular Surface Area
PPS	Preliminary Phytochemical Screening
rGyr	Radius of Gyration
RMSD	Root Mean Square Deviation
RMSF	Root Mean Square Fluctuation
SASA	Solvent Accessible Surface Area
WHO	World Health Organization

1. Introduction

Alzheimer's disease (AD) is a chronic, neurodegenerative, and incurable brain disease categorized by behavioral and cognitive deterioration by damage, constituting 60–80 % of individuals affected by dementia [1]. According to the Global Alzheimer Survey 2021, worldwide, the number of individuals with dementia exceeds 55 million, and this quantity is projected to triple, becoming 152 million by 2050. Consequently, AD is anticipated to become a fifth most predominant cause of death [2].

The pathophysiology of Alzheimer's disease (AD) brains shows a decrease in basal forebrain cholinergic neurons, leading to a reduction in choline acetyltransferase (ChAT), the enzyme that produces acetylcholine (ACh), which controls sleep cycles, memory, and learning [3]. In AD, the decrease in ChAT activity and ACh levels is closely associated with impaired cognition. In the synaptic cleft, acetylcholine and butyrylcholine signals are disrupted by two distinct enzymes acetylcholinesterase (AChE) and butyrylcholinesterase (BChE), respectively [4]. As a result, drugs that inhibit the breakdown of acetylcholine and butyrylcholine represent a therapeutic strategy to enhance cholinergic signaling in AD patients. The four FDA-approved drugs: Tacrine, Galantamine, Rivastigmine, and Donepezil work by inhibiting cholinesterase to increase acetylcholine levels, which are reduced in AD brains. Instead of curing the disease, these medications usually only offer fleeting, insufficient clinical alleviation and are accompanied by serious side effects such as diarrhea, vomiting, and liver damage [5].

The amyloid pathophysiology involves the formation of extracellular senile plaques composed of aggregates of amyloid beta (Aβ) peptides, which eventually cause brain shrinkage and neuron degradation, distinct from the cholinergic system [1]. Amyloid precursor proteins (APPs) are sequentially cleaved by beta-secretase (BACE-1) and gamma-secretase in brain regions to produce Aβ peptides. Aβ42 is believed to be released and accumulate as senile plaques in the initial phases of AD due to its limited soluble form and higher concentration of neurotoxic chemicals within amyloid plaques. Patients with a family connections of AD frequently have an greater brain Aβ42 ratio [6]. Preventing BACE-1 from cleaving APP is a key in component for inhibiting the production of Aβ. Furthermore, the abnormal accumulation of Aβ triggers the overproduction of AChE and BChE [7]. This results in the availability of elevated glutamate, an increase in the influx of Ca^{++}, upregulation of receptors for advanced glycation end products (RAGEs), and the overactivation of microglia and astrocytes, resulting in the production of neuroinflammatory cytokines such as TNF-α, IL-1, and IL-6 [8,9]. In AD, tau pathology involves the formation of intracellular neurofibrillary tangles (NFTs). These tangles result from the hyperphosphorylation of tau (p-tau) protein, which disrupts critical processes such as protein translation, axonal transport, and synaptic transmission in the brain [10]. Tau phosphorylation is regulated by protein kinase and phosphatase. Among these, glycogen synthase kinase 3β (GSK-3β) is associated with p-tau production. The production of NFTs is also influenced by Aβ. Aβ affects the activity of GSK-3β and other protein kinases, thereby inducing tau protein deposition and NFT formation [11]. The production of NFTs also contributes to increased glutamate levels. However, the rise in glutamate overstimulates the NMDA receptor, leading to NADPH oxidase (NOX)-mediated ROS production [12]. These ROS trigger the production of advanced glycation end products (AGEs). The interaction between AGEs and RAGEs forms a complex that can cross the BBB and activate GSK-3β as well as NF-kB. NF-κB activation further causes the upregulation of GSK-3β, which induces the phosphorylation of Tau (P-Tau) and its conversion to NFTs. Therefore, GSK-3β is a promising drug target for curing AD and inhibitors of GSK-3β can reduce abnormal Tau phosphorylation and amyloid protein production *in vitro* and in vivo, a promising disease-modifying therapy for AD. P-Tau also influences the expression of AChE, which interacts with PS-1 to overproduce Aβ, thus contributing to the progression of AD in a cyclic manner [11,13,14]. Therefore, based on the amyloid hypothesis, recent monoclonal antibody-based targeted therapies like Lecanemab (Leqembi) bind with high affinity to Aβ soluble protofibrils to halt the development of aggregation, while Aducanumab (Aduhelm) prefers binding to fibrils over protofibrils to remove amyloid-beta from the brain of Alzheimer's disease patients [15]. Unfortunately, these monoclonal antibody-based therapies can only be used by those who have moderate cognitive impairment. They do not stop or reverse the disease and do not improve cognitive abilities but may slow down its progression. Additionally, these antibody therapies have limitations such as brain edema or microhemorrhages, hypersensitivity reactions, headaches, diarrhea, falls, and high costs [15]. Inhibition of BACE-1 activity primarily reduces the production of Aβ.

However, clinical trials of BACE-1 inhibitors (verubecestat, lanabecestat, atabecestat, lanabecestat and atabecestat) have largely been unsuccessful due to serious liver-related adverse effects, toxicity, or a lack of clinical efficacy [16].Tideglusib, a GSK-3β inhibitor, was shown to reduce tau phosphorylation. However, in a double-blind, placebo-controlled Phase II trial, it failed to show clinical benefits for Alzheimer's disease [17]. The clinical efficacy of GSK-3β inhibitors in Alzheimer's remains under investigation. Since the pathophysiology of Alzheimer's disease is multifactorial, a promising approach would logically be to target multiple factors of the disease with a single drug, making this the best choice [18].

Traditional medicines that originate from natural sources are being studied as potential alternative treatments for AD. These medicines have garnered interest due to their diverse biological activities, unique structures, and safety for consumption, cost-effectiveness, minimal side effects, and ability to target multiple factors contributing to AD. These attributes make them appealing to the research and development of potentially novel drugs.

Argemone mexicana L. is a flowering plants consisting of the family of *Papaveraceae*. It is a prickly herbaceous plant with yellow juice, 0.3–12 m heights, thistle-like leaves, and flashy yellow flowers [19]. It is globally recognized as Mexican poppy and is known as Shyalkanta in Bangladesh. This plant is native to Mexico and uses its sap for eye diseases. For this, this plant is known as *A. mexicana*. It is considered an exotic weed and is exultant in almost every part of India and Bangladesh. It is widely used in indigenous Ayurvedic medication to treat dropsy, antimicrobial, yellowing of the skin eye disease, scabies, and dermatological illnesses [20]. The various components of these plants have therapeutic qualities that are beneficial for dealing with malignancies and chronic skin ailments. They are also utilized as emetics, anticipates, demulcents, diuretic drugs, and anti-inflammatory substances. The extract derived from the seeds, seed oil, and leaves treats diarrhea, ulcers, asthma, snake toxic exposure, and scorpion bites. Additionally, it is believed to aid in sustaining proper circulation of blood and blood cholesterol levels in humans. In Siddha medicine, the leaves and black pepper cure diabetes. A thorough investigation has been carried out on the pharmacological properties of this plant, including antimicrobial, antidiabetic, anticancer, antioxidant, anti-inflammatory, anthelmintic, larvicidal, hepatoprotective, analgesic, and wound healing activities [21,22]. However, neuropharmacological activities such as analgesic, locomotor, and muscle relaxant effects of the whole plant of *A. mexicana* have been reported [19]. The compounds found in *A. mexicana* have not yet been discovered for treating AD.

In this research, we wish for purpose to comprehensively and thoroughly evaluated the anti-AD prospective and discover novel compounds from *A. mexicana* leaves and flowers extracts as potential drug candidates that might work through a multi-target-directed ligand (MTDL) strategy. The all-encompassing methodologies consists of conducting *in vitro* assessments of antioxidant and anti-acetylcholinesterase and anti-butyrylcholinesterase activity assays and *in silico* evaluation of molecular docking simulation, MMGB-SA analysis, pharmacokinetics, drug-likeness, and toxicity properties, in addition, simulations based on molecular dynamics are employed to validate the efficacy of the lead compounds. These strategies aim to identify a solitary molecule with the capacity to modulate multiple vital targets or pathways, such as AChE and BChE in the cholinergic pathway, β-secretase BACE-1) in the amyloidogenic pathway, and GSK-3β in the Tau pathway pertaining to AD. The findings from this research are anticipated to offer valuable insights regarding the prospective medicinal applications of *A. mexicana* in combating AD, and are likely to contribute to the development of innovative multi-target directed bioactive compounds to fight against Alzheimer's disease.

2. Materials and methods

2.1. Chemicals and reagents

Ethyl acetate, methanol, and ethanol, Mayer's reagents, Fehling's reagents A and B, H_2SO_4, Na_2HPO_4, NaH_2PO_4 and $K_2S_2O_8$, H_2O_2, $FeCl_3$ were obtained from Germany. L-ascorbic acid, NaOH, NaCl, Sodium nitroprusside, Tris-base, and chloroform were procured from India. HCL from Thailand. Pyridine from UK. DPPH, acetylcholinesterase, acetylcholine iodide, butyrylcholinesterase, butyrylthiocholine iodide, DTNB, and donepezil hydrochloride bought from USA.

2.2. Plant materials collection

The leaves and flowers of the *Argemone mexicana* L. plant were collected at Churamonkathi, Jashore, and taxonomically distinguished by Professor Dr. A. M Swaraz, Department of Genetic Engineering and Biotechnology, Jashore University of Science and Technology, Bangladesh. The plant voucher specimen number DACB 65146 was deposited at the National Herbarium, Dhaka, Bangladesh.

2.3. Plant extracts preparation

The plant materials were extracted in a manner consistent with the previously described procedure, with minor modifications [23]. The collected plant materials were rinsed and air-dried in an air-conditioned setting at 25 °C. The dried plant material was then finely pulverized in a grinder into a powder, which was subsequently sieved with a mesh size of 1 mm (Sieve No. 10/44). A total of 75 g of powdered plant material was divided into three 250-mL conical flasks. Each flask contained 125 mL of methanol, ethanol, and ethyl acetate, respectively. After 72 h of continuous agitation at 250 rpm in a shaking incubator set at 37 °C, the mixtures underwent 15 min of centrifugation at 8000 rpm. The resulting supernatants were filtered using filter paper, and the filtered liquid was evaporated using a vacuum rotary evaporator. Once the water had completely evaporated at ambient temperature, the crude extract was stored in a freezer at 4 °C.

2.4. Gas chromatography-mass spectrometry (GC-MS) analysis

GC-MS was operated following a previously described method by Rahat et al. with little bit alterations [24]. The phytoconstituents of MEAMLF, EEAMLF and EAEAMLF extract were used to identify by the Shimadzu triple-quad GCMS- TQ8040. The stationary phase was the Rtx-5MS capillary column, which has an internal diameter of 30m and a thickness of 0.25 m. The mobile phase consisted of helium gas. Dedicated software was attached to the GC-MS machine and controlled the column oven temperature at 1, 2, and 7 min, settling at 50, 200, and 300 °C, respectively. The flow rate was maintained at 1 mL/min, and 1 μL of each of the samples was injected. A total of 40 min of experiment ran with the sample injector temperature set at 250 °C. The instrumental criteria were established as inner face and ion source temperature was 250 and 230 °C, with a 2000 scan mode of 50–600 (m/z) scanning range, and it was scanned with an interval of 0.3 s. Through the comparison of spectrum pattern and retention time, phytochemicals have been determined. The National Institute of Standards and Technology (NIST) database was used to curate compounds. All samples underwent triplicate technical and biological replication for each sample preparation. For determining the phytochemical compound content in an extract as a percentage, the peak area of a specific ingredient was compared to the overall peak area of all other peaks.

2.5. Computational study

2.5.1. Protein retrieval and preparation

The 3D x-ray crystallography models of AChE (PDB id: 4EY7), BChE (PDB id: 1P0I), BACE-1 (PDB id: 4JPE), and GSK-3β (PDB id: 1Q5K) have been retrieved from the RCSB protein data bank [25–28]. The protein preparation wizard in the Schrodinger suite version 2020-3 was used to separate bound ligands, heteroatoms, water molecules, and co-factors from the co-crystallized family proteins [29]. Proteins were prepared by bond orders assessment, zero-order bonds creation to metals, and double sulfide bonds utilization for filling the side chains. The protein crystal configuration was refined and curtailed using the OPLS-3e energy field.

2.5.2. Compounds library preparation

Naturally, originated plant-based phytochemicals proliferate the drug discovery process, which has a distinct chemical species. The GC-MS analysis of EEAMLF, EAEAMLF, MEAMLF, and IMPPAT databases identified 196 unique compounds. The phytoconstituents are downloaded using PubChem database in 3D SDF format. To process and prepare the bioactive ligand molecules, Maestro Schrödinger Ligprep wizard was used. A minimal structure for the ligand high-energy ionization states was obtained using Epik version 5.3 at pH 7.0 ± 2. By determining prospective chiral centers on each molecule and employing the OPLS3e force field to generate 236 possible stereoisomers, a further minimization process was performed.

2.5.3. Interaction site and receptor grid generation

A protein's binding pocket is a region in which certain amino acid residues allow the protein to make contact with ligand molecules. As in the computational drug discovery procedure, BS identification plays a principal role in molecular docking study by generating connection points with the amino acids of proteins that provide appropriate catalytic surroundings that ensure the significant binding efficiency of protein ligands. In this study, for AChE, BChE, BACE-1, and GSK-3β using the co-crystallized reference ligand E20 (CID 1150567), NAG (CID 24139), 1M7 (CID 66684136), and TMU (CID 448014) respectively attaching residues at the position were selected as the binding site to generate the grid box depicted at Table S1 and using the Schrodinger maestro 2020-3 to prepare the protein. Using the OPLS3e force field, the van der Waals radii scaling factor of 1.0, and a charge cutoff at 0.25, the grid was adjusted to generate a cubic box around the binding region of the receptor protein.

2.5.4. Standard precision (SP) molecular docking

Molecular docking is useful techniques in computational research, which predicts structural configuration of bonds, the strength of interactions, and binding nodes involving in proteins and ligands. In this study, standard precision (SP) molecular docking procedure was conducted for each receptor individually by implementing Glide v11 module in the Schrodinger suite to determine the interaction mode. An assessment was made of the compounds that exhibited the greatest binding affinities about the control drugs CID 3152 (Donepezil). This methodology facilitates the most suitable orientations and interactions with the highest binding affinity among the receptor and ligand molecules. The Maestro Schrodinger visualization tools was employed for the visualization of protein-ligand binding site and associated different chemical bonding.

2.5.5. MM-GBSA analysis

The MM-GBSA approach was utilized to calculate the binding-free energies of ligands bound to proteins. Protein-ligand binding scores analysis is to identify lead compounds that provide an accurate and continuous affinity. One way to assess the accuracy of energy calculation approaches, MM-GBSA is through the validation of the docking mechanism. To figure out the free energy of binding between the AChE, BChE, BACE-1, GSK-3β protein, and the selected ligands and control drug, an MM-GBSA study was conducted by the Desmond 11.3 v3.6 package. With OPLS 2005 and other default parameters, we can predict the G bond, the Coulomb energy, the H-bond energy, the lipophilicity energy, the Pi-Pi packing energy, the Solv GB (Generalized Born Electrostatic Solution Energy), and the van der Waals interaction energy. The energy expression integrates these elements in order to convey the binding energies for receptor-ligand complexes.

2.5.6. Analyses of pharmacokinetics (PK) and toxicity properties

A drug's PK properties can be defined as preclinical safety measurements that include absorption, distribution, metabolism, and excretion (ADME) to reduce the likelihood of pharmacological failure. In drug discovery and development procedures, pharmacokinetics (ADME) properties are very important features that reduce the later-stage clinical failure that is so promising. The SwissADME server was applied to assess the pharmacological properties of the ligand molecules. A small molecule can damage any organ in the human body by showing cytotoxicity, carcinogenicity, hepatotoxicity, immune toxicity, and mutagenicity, so toxicological properties checking is a vital element for drug discovery. A free web server ProTox-II was utilized to demonstrate the toxic properties in lead compounds, predicted LD_{50}, and toxicity classes of selected compounds.

2.5.7. Molecular dynamics (MD) simulation study

MD simulations was assessed the intricate protein-ligand structure by constructing a artificial bimolecular environment to assess the binding state of the chosen ligand molecules and the interaction stiffness of the receptor protein active site cavity. Furthermore, by simulating the complex structure at a molecular scale, MD simulations help to predict thermodynamic stability, average atom distance, and molecule fluctuation [24]. To determine the physical movements associated with the protein-ligand complex alongside the highest binding score of AChE, BChE, BACE-1, and GSK-3β, a 250 ns MD simulation was performed using the maestro Desmond v3.6 program. The respective protein-ligand complexes were generated from the molecular docking output file and each of the complex was surrounded with a cubic box ranging from 10 Å × 10 Å × 10 Å at X, Y, and Z co-ordinates. A three-site transferable intermolecular potential (TIP3P) water program is additionally addressed to sustain a predetermined volume inside an orthorhombic box framework and by applying simple point-charge (SPC) water models to confirm the distinctive system volume throughout the simulation. Na + ions having an amount of 0.15 M were applied to eliminate the environment, and an OPLS3e force field was implemented for conducting this simulation. Each of the complex was relaxed primarily, than a final production cycle was executed with 100 ps recording intervals utilizing an energy value of 1.2. At constant pressures (101325 Pa) and temperatures of 310K, a natural time and pressure (NPT) ensemble minimized the complex of the protein and ligand system. Significantly, numerous variables have been established to measure the dynamic and stability aspects of these complexes. These parameters include root mean square deviations (RMSD) for proteins and ligands, root mean square fluctuations (RMSF) for proteins, gyration radiuses of gyration (rGyr), molecular surface area (MolSA), solvent accessible surface area (SASA), hydrogen bonds, protein-ligand interactions, and simulation snapshots.

2.6. In vitro antioxidant assay

2.6.1. In vitro scavenging of DPPH assay

The DPPH scavenging assay was used to assess the antioxidant activity of MEAMLF, EEAMLF, and EAEAMLF, following the methods of Akhtar et al. [30]. Methanol was used to prepare individual stock solutions of the respective plant extracts, ascorbic acid, and DPPH, each at a concentration of 1.0 mg/mL. In this assay, 40 μL of serially diluted extracts and ascorbic acid at concentrations of 200, 100, 50, 25, 12.5, 6.25, 3.125, and 1.561 μg/mL were added to a 96-well microplate separately. Then, 6 μL of the DPPH stock solution was added to each well to reach a final concentration of 30 μg/mL. Finally, 154 μL of methanol was added to each well to achieve a total volume of 200 μL. The negative control sample was prepared with 6 μL of 1 mg/mL DPPH and 194 μL of methanol. The reaction mixtures were incubated at room temperature for 30 min. Absorbance was measured at 514 nm using an ELISA reader, the Multiskan SkyHigh Microplate Spectrophotometer (Thermo Fisher Scientific, USA). Three independent experiments were conducted for each analysis, and calculations were performed using the average absorbance. The DPPH scavenging effect was estimated using the following formula:

$$\%\ \text{DPPH scavenging activity} = \frac{(\text{Abscontrol} - \text{Abssample or Absascorbic acid})}{\text{Abscontrol}} \times 100$$

The sample's and controls specific absorbance's are $Abs_{control}$ and Abs_{sample}. $Abs_{ascorbic\ acid}$ is the ascorbic acid absorbance. The IC_{50} of the various extracts and ascorbic acid was calculated using Microsoft Excel, with the level of inhibition displayed across the amount of the substance. IC_{50} was calculated at y = 50 using the formula y = mx + c, where x is the IC_{50} and y is the 50 positions of the curve.

2.6.2. In vitro H_2O_2 scavenging assay

The antioxidant measurement of MEAMLF, EEAMLF, and EAEAMLF was conducted using the H_2O_2 scavenging assay, following the method described earlier with slight modifications [31]. Briefly, a 0.4 M solution of H_2O_2 was prepared using phosphate-buffered saline (PBS) (pH 7.4). In this assay, 40 μL of serially diluted extracts and ascorbic acid at concentrations of 200, 100, 50, 25, 12.5, 6.25, 3.125, and 1.561 μg/mL were added to a 96-well microplate separately. Then, 10 μL of the 0.4 M H_2O_2 stock solution was added to each well to reach a final concentration of 20 mM H_2O_2. Finally, 150 μL of PBS (pH 7.4) was added to each well to achieve a total volume of 200 μL. The negative control sample was prepared with 10 μL of 0.4 M H_2O_2 solution and 190 μL of PBS (pH 7.4). The reaction mixtures were incubated at room temperature for 10 min. After incubation, the absorbance was measured at 230 nm using an ELISA reader, the Multiskan SkyHigh Microplate Spectrophotometer (Thermo Fisher Scientific, USA). The H_2O_2 scavenging capability of the extracts and ascorbic acid was estimated using the following formula:

$$\%\ H_2O_2\ \text{scavenging activity} = \frac{(\text{Abscontrol} - \text{Abssample or Absascorbic acid})}{\text{Abscontrol}} \times 100$$

$Abs_{control}$ and Abs_{sample} are the absorbances of the control and individual extract correspondingly. $Abs_{ascorbic}$ acid is the absorbance of ascorbic acid. Microsoft Excel has been used to calculate the value of the IC_{50} for each extract and ascorbic acid, as described in the DPPH assay.

2.6.3. In vitro anti-acetylcholinesterase and anti-butylthiocholineesterase enzyme inhibition assay

Inhibition of AChE activity was measured using a modified 96-well microplate assay based on Ellman's method [27]. AChE hydrolyzes the substrate acetylthiocholine, resulting in the product thiocholine, which reacts with Ellman's reagent (DTNB) to produce 2-nitrobenzoate-5-mercaptothiocholine and 5-thio-2-nitrobenzoate, which can be detected at 412 nm. In this assay, 50 μL of serially diluted extracts and donepezil at concentrations of 200, 100, 50, 25, 12.5, 6.25, 3.125, and 1.561 μg/mL were added to a 96-well microplate separately, making a total volume of 250 μL in each well. Each sample well was filled with 125 μL of 2 mM DTNB (5,

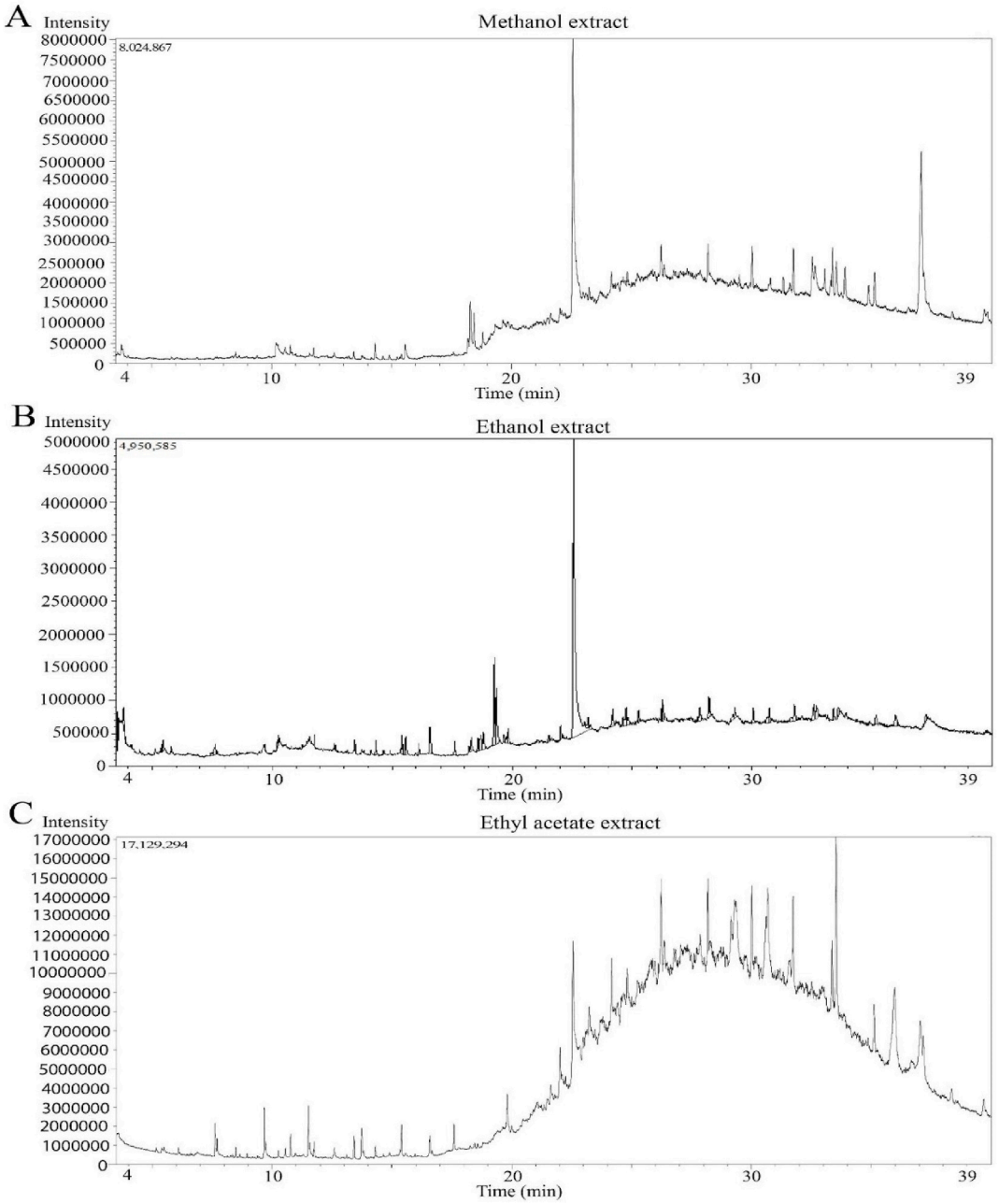

Fig. 1. GC-MS chromatograms of phytoconstituents were annotated in MEAMLF, EEAMLF, and EAEAMLF. (A) MEAMLF, (B) EEAMLF and (C) EAEAMLF.

5-dithio-bis-(2-nitrobenzoic acid)) to a final concentration of 1 mM DTNB dissolved in 20 mM Tris-HCl (pH 8.0) buffer and 25 μL of 10 U/mL AChE dissolved in 20 mM Tris-HCl (pH 8.0) buffer to a final concentration of 1 U/mL. The reaction mixtures were properly mixed using a pipette and incubated at 25 °C for 15 min. After incubation, 25 μL of 2.5 mM AChI in deionized water, to a final concentration of 0.25 mM, was added as the substrate to the mixtures. The reaction mixtures in each well were properly mixed using a pipette and then incubated again for 15 min at 25 °C. The negative control contained 50 μL of 20 mM Tris-HCl (pH 8.0) buffer instead of the extract, 125 μL of 2 mM DTNB, and 25 μL of 10 U/mL AChE, incubated at 25 °C for 15 min, followed by adding 25 μL of 2.5 mM AChI and additional incubation at 25 °C for 15 min. In this study, donepezil was employed as a control drug. In the anti-BChE enzyme inhibition assay, all conditions and reaction mixtures were the same as in the anti-AChE enzyme inhibition assay, except BChE and BChI were used instead of AChE and AChI. The absorbance was measured at 412 nm using an ELISA reader, the Multiskan SkyHigh Microplate Spectrophotometer (Thermo Fisher Scientific, USA), and the percentage of enzyme inhibition was calculated as follows:

$$\%\ \text{Inhibition} = \frac{\text{Abscontrol} - \{(\text{Abssample} - \text{Abs only plant extract})\}\ \text{or}\ \text{Abspositive control}}{\text{Abscontrol}} \times 100$$

Where, $Abs_{control}$ is the enzyme's action in the absence of an extract and Abs_{sample} is the activity of enzyme with respective extract. $Abs_{positive\ control}$ represents the activity of standard drug donepezil. The IC_{50} value of extracts and reference drug was determined using MS Excel by illustrating a curve of % inhibitions and correlating test sample amounts with this equation: $y = ax + b$. The IC_{50} was calculated at the curve's $y = 50$ location.

3. Results

3.1. GC-MS analysis

GC-MS analysis metabolically annotated 70, 34, and 66 phytoconstituents in MEAMLF, EEAMLF, and EAEAMLF, respectively. The relative percentage amounts of each respective extract peak area compared with the total area from the GC-MS chromatogram are displayed in Fig. 1A, B and 1C. The structure, name, and formula of the phytochemicals along with retention time (RT), peak area (percentage), compounds CID, canonical smiles, and nature of the phytochemicals depicted in Tables S4, S5, and S6. With a retention period of 39 min, the respective extracts of each phytochemical comprised phenols, terpenoids, steroids, sterols, esters, alkaloids, alkanes, amines, carbonic acid, carboxylic acid, ethers, esters, hydrocarbons, fatty alcohols, fatty aldehydes, fatty acids, ketones, methoxyphenols, oleic acids, phthalates, and sugar alcohols. In our GC-MS analysis, seven common compounds were found in MEAMLF and EEAMLF, five common compounds were found in EEAMLF and EAEAMLF, and thirteen common compounds were found in MEAMLF and EAEAMLF. From the GC-MS analysis, we annotated 170 compounds, with 147 unique compounds identified from the three respective extracts. Their abundance in MEAMLF was ordered as follows: amide (20.22 %) > steroid (14.09 %) alkane (8.86 %) > acid (8.3 %) > alkaloids (3.7 %) > ester (4.37 %) > ketone (3.21 %) > diterpene (1.8 %) > alcohol (1.7 %) > phenol (1.6 %) > organo fluorine (1.48 %) > ether (1.4 %) > carbohydrate (1.23 %) > aldehyde (0.65 %) > amine (0.65 %) > epoxide (0.54 %) piperazine, accordingly. The abundance of phytocompounds content in EEAMLF was as follows: amide (46.43 %) > ester (15.37 %) > acid (9.91 %) > alkane (6.17 %) > alcohol (5.71 %) > alkaloid (4.04 %) > amine (3.25 %) ether (2.82 %) > alkane (1.16 %) > diterpene (0.93 %) > aromatic (0.86 %) > glucose (0.8 %). However, the relative content of phytocompounds in EAEAMLF was as follows: alkane (39.6 %) > ester (19.21 %) > acid (13.64 %) > acyl (8.89 %) > alcohol (3.91 %) > terpene (3.09 %) > aldehyde (2.63 %) > ether (2.63 %) > alkane (2.6 %) > phenol (1.68 %) > amine (0.51 %) > ketones (0.53 %) > aldimine (0.6 %). The major compounds found in MEAMLF were 9-Octadecenamide, (Z)- (20.22 %), Cholest-5-en-3-ol, (3.alpha.)-, TMS derivative (13.49 %), Allocryptopine (2.17 %), Cyclopentadecanone, 2-methyl- (1.95 %), and Octatriacontyl trifluoroacetate (1.48 %). The most prevalent phytocompounds in EEAMLF were 9-Octadecenamide, (Z)- (45.44 %), 9,12-Octadecadienoic acid (Z,Z)- (7.29 %), Ethyl Oleate (5.56 %), protopine (2.38 %), 11-Methyltricosane (1.93 %), and Oxirane, tetradecyl- (1.79 %). The most predominant phytocompounds in EAEAMLF were Octatriacontyl trifluoroacetate (8.04 %), octadecyl ester (6.6 %), 9-Octadecenamide, (Z)- (6.5 %), Dodecane, 1,2-dibromo- (3.97 %), Eicosyl isopropyl ether (1.9 %), and 1-Hentetracontanol (1.77 %).

3.2. Computational study

3.2.1. Molecular docking study

An investigation using molecular docking was conducted to comprehend the molecular binding affinities of the assigned macromolecules with the best intramolecular small biological compounds from *Argemone Mexicana*. It needs to be done to determine the

Table 1
Multitargeting ability and molecular docking scores of the choosing molecules with AChE, BChE, BACE-1, and GSK-3β.

Compound	Docking Score (Kcal/mol)			
	AChE	BChE	BACE-1	GSK-3β
Protoberberine (CID 114943)	−11.2	−6.969	−6.122	−7.252
Protopine (CID 4970)	−10.864	−6.468	−5.61	−5.776
Codeine (CID 5284371)	−10.204	−6.338	−5.654	−5.465
Donepezil (CID 3152)	−10.171	−6.227	−5.521	−5.146

binding energy and affinity between ligand-protein to ascertain the molecular makeup of the protein-ligand complex. A total of 196 phytochemicals were docked with AChE, BChE, BACE1, and GSK3β receptors. The compounds with the negative maximum binding score exceeding −5.00 kcal/mol are screened and depicted at Tables S7, S8, S9, and S10. In this study, AChE-compound complexes exhibited the negative highest docking score than the control drug donepezil. The docking score revealed that our nominated plant's top three compounds, CID 114943, CID 4970, and CID 5284371, showed the binding score of −11.2 Kcal/mol, −10.864 kcal/mol, and −10.204 kcal/mol respectively whereas donepezil showed −10.171 kcal/mol. From AChE receptor docking, we were well-informed about these three compounds and contemplated the docking score with other elected receptors. Here, BChE, BACE1, and GSK-3β also

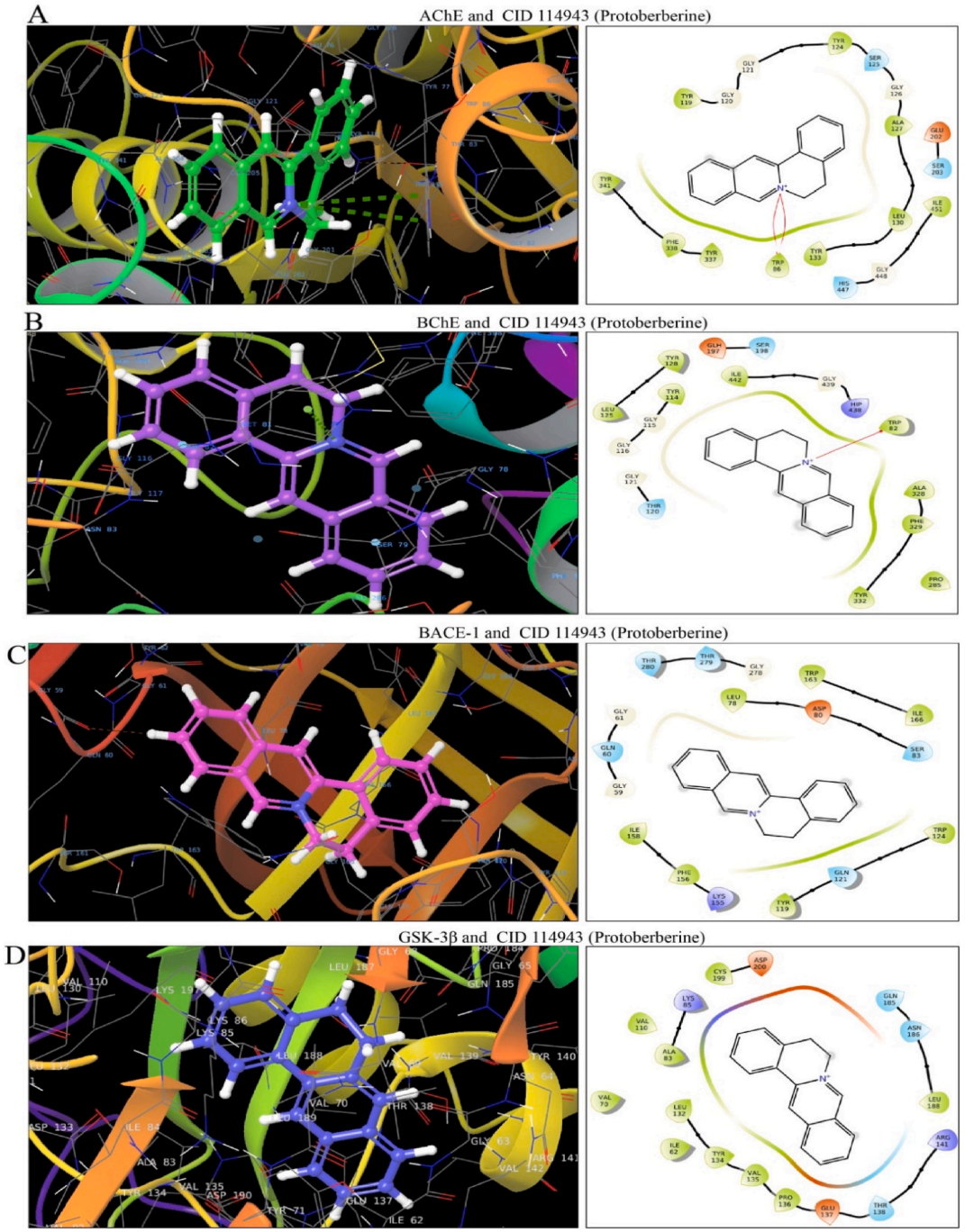

Fig. 2. Multi-modal molecular docking interaction of protoberberine and neuronal pathologic targets. (A) AChE and CID 114943 (Protoberberine) (B) BChE and CID 114943 (Protoberberine), (C) BACE-1 and CID 114943 (Protoberberine), and (D) GSK-3β and CID 114943 (Protoberberine). Left side is 3D, right side is 2D of protein-ligand.

provided higher docking scores for all three compounds compared to donepezil, indicating a multi-targeting ability of all three compounds as depicted in Table 1.

3.2.2. Protein-ligand interaction analysis

The Maestro package from the Schrödinger software was employed for demonstrating how molecules interact between receptors and ligands, encompassing bonds composed of hydrogen, electrostatic bonds, polar bonds, van der Waals bonds, glycine bonds,

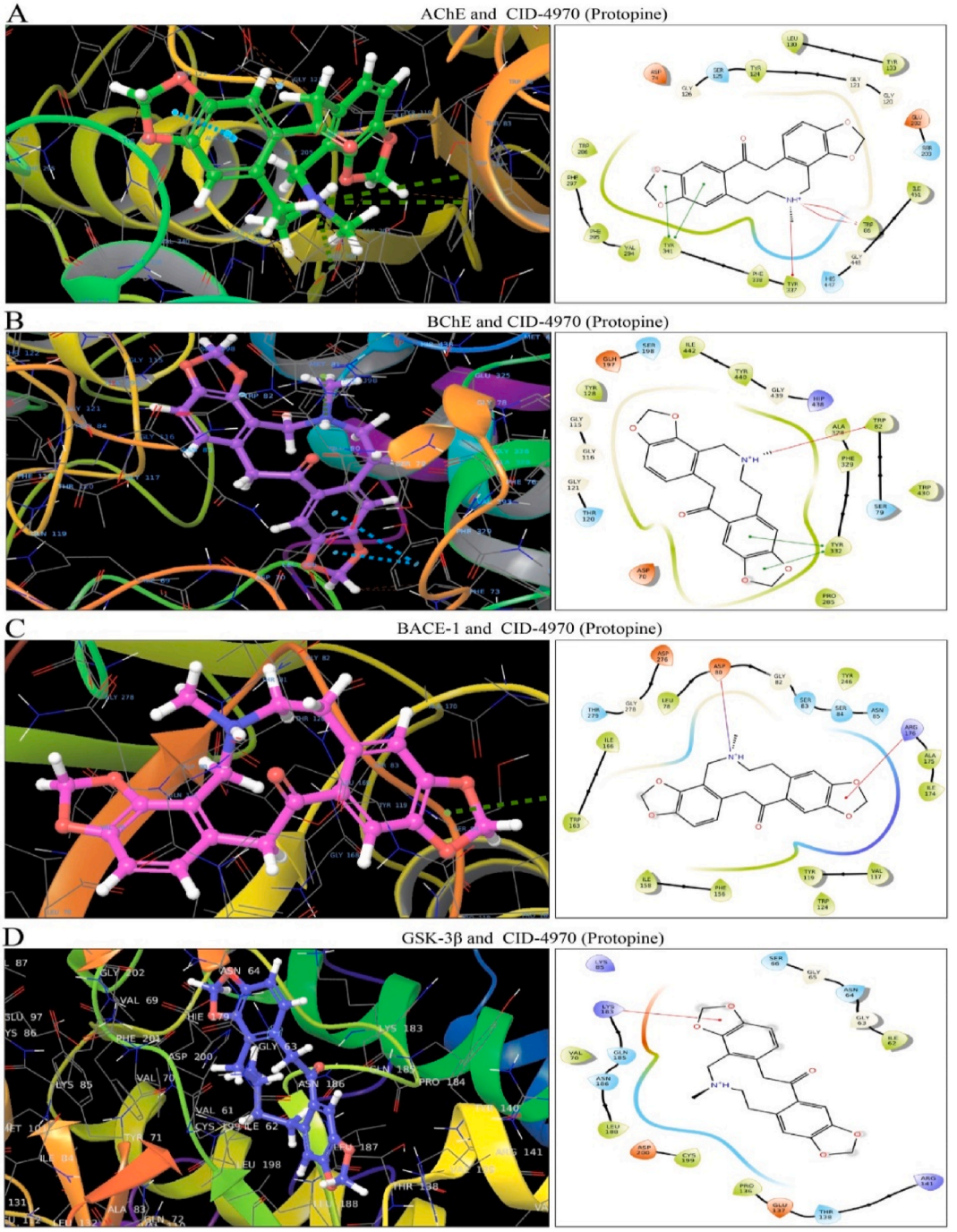

Fig. 3. Multi-modal molecular docking interaction of protopine and neuronal pathologic targets. (A) AChE and CID 114943 (protopine) (B) BChE and CID 114943 (protopine), (C) BACE-1 and CID 114943 (protopine), and (D) GSK-3β and CID 114943 (protopine). Left side is 3D, right side is 2D of protein-ligand.

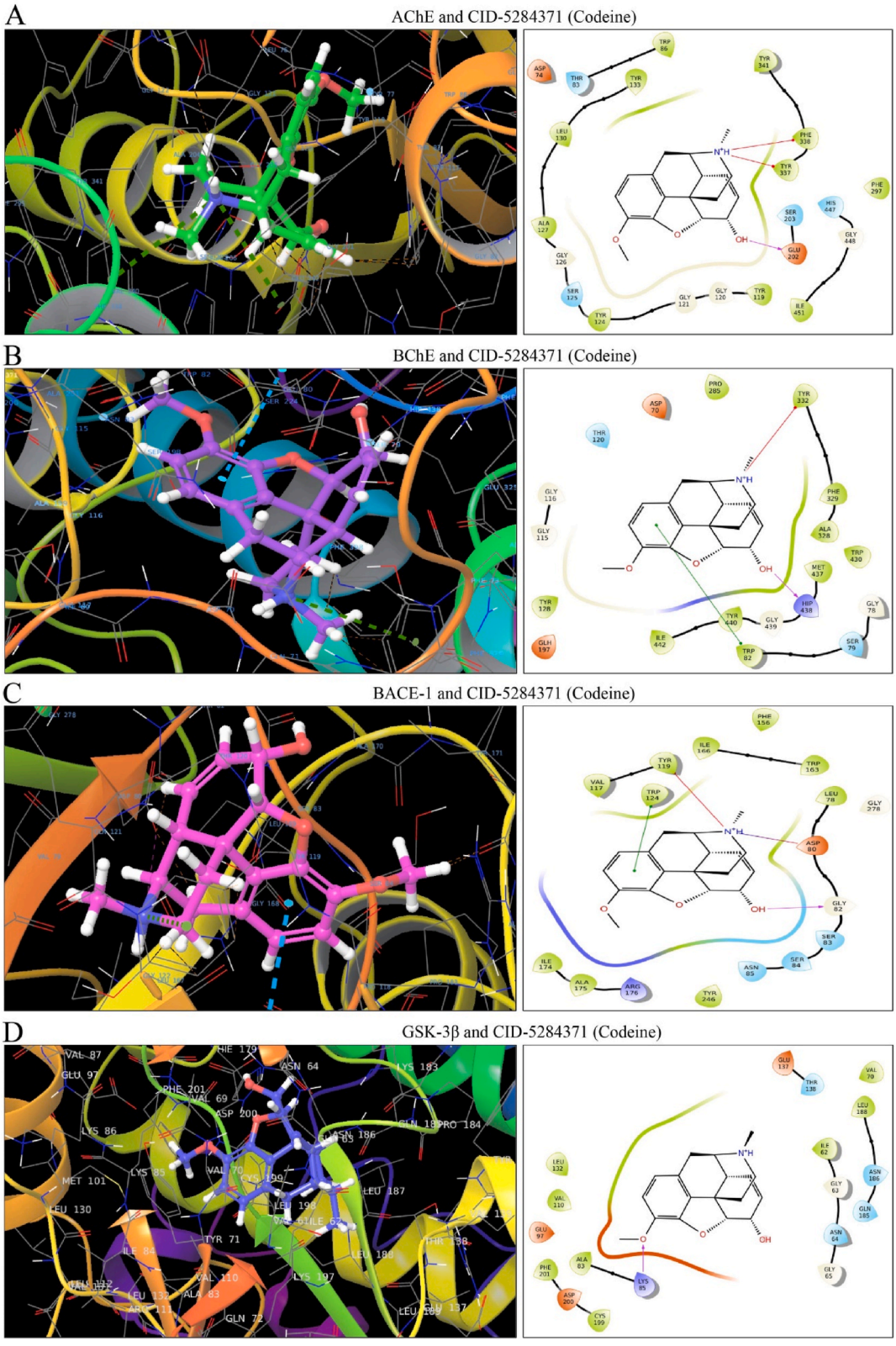

Fig. 4. Multi-modal molecular docking interaction of codeine and neuronal pathologic targets. (A) AChE and CID 114943 (codeine) (B) BChE and CID 114943 (codeine), (C) BACE-1 and CID 114943 (codeine), and (D) GSK-3β and CID 114943 (codeine). Left side is 3D, right side is 2D of protein-ligand.

covalent bonds, ionic bonds, and hydrophobic bonds. All the bonding symbolized that the selected compounds strongly bind with the respective receptor illustrated in Figs. 2–5, and in Table S11. The leading three compounds and the control ligand interacted with several commonly occurring amino acids that were present during the docking process of AChE, BChE, BACE1, and GSK-3β. In AChE, TRP86, GLY120, GLY121, PYR124, TYR133, GLU202, SER203, TYR337, PHE338, TYR341, HIS447, GLY448, ILE451 are the common interacting residues whereas, in BChE, TRP82, GLY115, GLY116, THR120, TYR128, GLU197, PRO285, ALA328, PHE329, TYR332, HIS438, GLY439, and ILE442 are the common interacting residues. In BACE-1, the common interacting residues include LEU78, ASP80, SER83, TYR119, TRP124, PHE156, and TRP166. In GSK-3β, the common interacting residues comprise ILE62, VAL70, LYS85, GLU137, THR138, GLN185, ASN186, LEU188, CYS199, and ASP200. Multiple common interacting bonding and non-bonding interactions are similar with the control drugs that denoted these specific amino acids are the active site residues for the respective protein. Hydrophobic interactions significantly enhance the binding affinity of the docked complex within a specific solvent environment, driven by entropy-based forces. These hydrophobic interactions are crucial for folding proteins, maintaining their stability and biological activity, and reducing undesirable interactions with water. The table shows that the respective receptors, when complexed with selected compounds, exhibit many hydrophobic bonds.

3.2.3. Post docking MM-GBSA analysis

To ascertain the endpoint bind free energy of the protein-ligand complex after molecular docking, the MM-GBSA methodologies have been designated. The MM-GBSA of AChE, BChE, BACE-1, and GSK-3β protein in complex with the established drug CID 3152 (donepezil) and the three specific molecules CID 114943, CID 4970 and CID 5284371 disclosed the greater or instead comparable values of net negative bound free energy when they came into contact with their respective apoprotein. Upon completion of the docking, the intricate investigation using MM-GBSA for the designated compounds' constrained energies is depicted in Figs. S5 and S6, and Table 2. The compound CID 114943 binding free energy is estimated to be approximately (−67.65, −55.593, −53.31, a nd −39.807 kcal/mol) for AChE, BChE, BACE-1, and GSK-3β, respectively. This value comprises various energy components, including Coulombic interaction energy (ΔG_bind Coulomb) of (−42.23, 31.05, −25.42, and 107.40 kcal/mol), covalent interaction energy (ΔG_bind Covalent) of (0.442, 0, 0.45, and 0.34 kcal/mol), hydrogen bonding energy (ΔG_bind Hbond) of 0.21, −0.19, −0.94, and −0.69 kcal/mol), lipophilic interaction energy (ΔG_bind Lipo) of (−0.21, −0.19, −0.94, and −0.69 kcal/mol), packing interaction energy (ΔG_bind Packing) of (−9.54, −7.51, −1.18, −0.57 kcal/mol), solvation energy (ΔG_bind Solv GB) of (46.16, −23.63, 30.40, and −99.38 kcal/mol), and van der Waals interaction energy (ΔG_bind vdW) of (−39.65, −35.61, −30.47, and −32.70 kcal/mol), respectively (Figs. S5 and S6). The compound CID 4970 shows binding free energy (−45.38, −48.46, −48.08, and −32.89 kcal/mol) for AChE, BChE, BACE-1, and GSK-3β, accordingly. It is comprised of Coulombic interaction energy of (−60.38, −5.23, −38.04, and 36.42 kcal/mol), covalent interaction energy of (3.14, 0, 1.08, and 3.77 kcal/mol), hydrogen bonding energy of (−0.09, −0.35, −0.09, −0.12 and kcal/mol), lipophilic interaction energy of (−35.85, −26.98, −21.02, and −12.83 kcal/mol), packing interaction energy of (−5.41, −4.15, −1.91, and −0.17 kcal/mol), solvation energy of (99.87, 37.26, 52.845, and −23.31 kcal/mol), and van der Waals interaction energy of (−46.66, −49.03, −40.92, and −36.64 kcal/mol) (Figs. S5 and S6). The binding free energy for CID 5284371 is approximately (−38.18, −49.24, −45.95, and −21.94 kcal/mol) when complexed with the AChE, BChE, BACE-1, and GSK-3β, correspondingly. This value includes Coulombic interaction energy of (−52.87, −1.54, −46.43, and 53.76 kcal/mol), covalent interaction energy of (3.66, 0, 7.43, 3.31 kcal/mol), hydrogen bonding energy of (−1.08, −0.87, −0.54, and −0.79 kcal/mol), lipophilic interaction energy of (−31.56, −25.94, −22.80, and −16.85 kcal/mol), packing interaction energy of (−2.28, −3.18, −1.22, and −0.008 kcal/mol), solvation energy of (88.79, 22.05, 48.77, and −40.70 kcal/mol), and van der Waals interaction energy of (−42.82, −39.76, −31.15, and −20.65 kcal/mol) (Figs. S5 and S6). Finally, the calculated binding free energy for control drug CID 3152 complexes with the AChE, BChE, BACE-1, and GSK-3β were (−65.63, −56.76, −51.26, and −41.37 kcal/mol), individually. It consists of Coulombic interaction energy of (−58.45, −1.98, −30.42, and 46.21 kcal/mol), covalent interaction energy of (1.01, 0, 1.85, and 6.43 kcal/mol), hydrogen bonding energy of (−0.22, −0.20, −0.84, and −0.44 kcal/mol), lipophilic interaction energy of (−43.05, −32.18, −24.53, −20.69 kcal/mol), packing interaction energy of (−7.84, −4.42, −1.55, and −0.10 kcal/mol), solvation energy of (91.21, 30.93, 50.04, and −31.75 kcal/mol), and van der Waals interaction energy of (−58.27, −48.91, −45.79, and −41.02 kcal/mol). In comparison to the control medication, these energy values demonstrated a more sustained interaction with each target protein. The findings were provided for the three specified compounds that displayed considerable contribution from a variety of aspects of different interacting bonds. These are the contributions of van der Waals interacting energy, pi-pi packing correction, coulomb energy, hydrogen bonding energy, lipophilicity energy, and generalized born electrostatic solvation energy. The result mentioned that the three chosen compounds can attach to the protein's attachment site for a prolonged duration and impede the activity of the target protein.

3.2.4. Pharmacokinetics (PK) and toxicity profiling

Assessing gastrointestinal (GI) absorption and blood-brain barrier (BBB) penetrability reflects favorable pharmacokinetic characteristics that screen potential drugs with a low chance of clinical drug failure for neurodegenerative diseases. In this study, we conducted GI absorption and BBB analysis on the three selected ligands with control drugs shown in Table 3 and all the compounds' GI and BBB screening is depicted in Table S13. All the selected compounds exhibited high GI absorption and BBB permeability, as the permeability of any drug through the BBB is critical aimed at its effectiveness in reaching the brain. It was observed that ligands adhered to Lipinski's rules, which outline specific properties of a lead compound. In this study, there is no Lipinski's rule violation, which allows for at least two violations to be acceptable. The CID 114943 showed no hydrogen bond acceptor, but the other two, CID 4970 and CID 5284371, have 6 4, respectively. Meanwhile, donepezil has four acceptors but no donor of hydrogen bonds. In contrast, only CID 4970 had one hydrogen bond donor (Table 3). The Log S score of a compound indicates its water solubility as a drug or

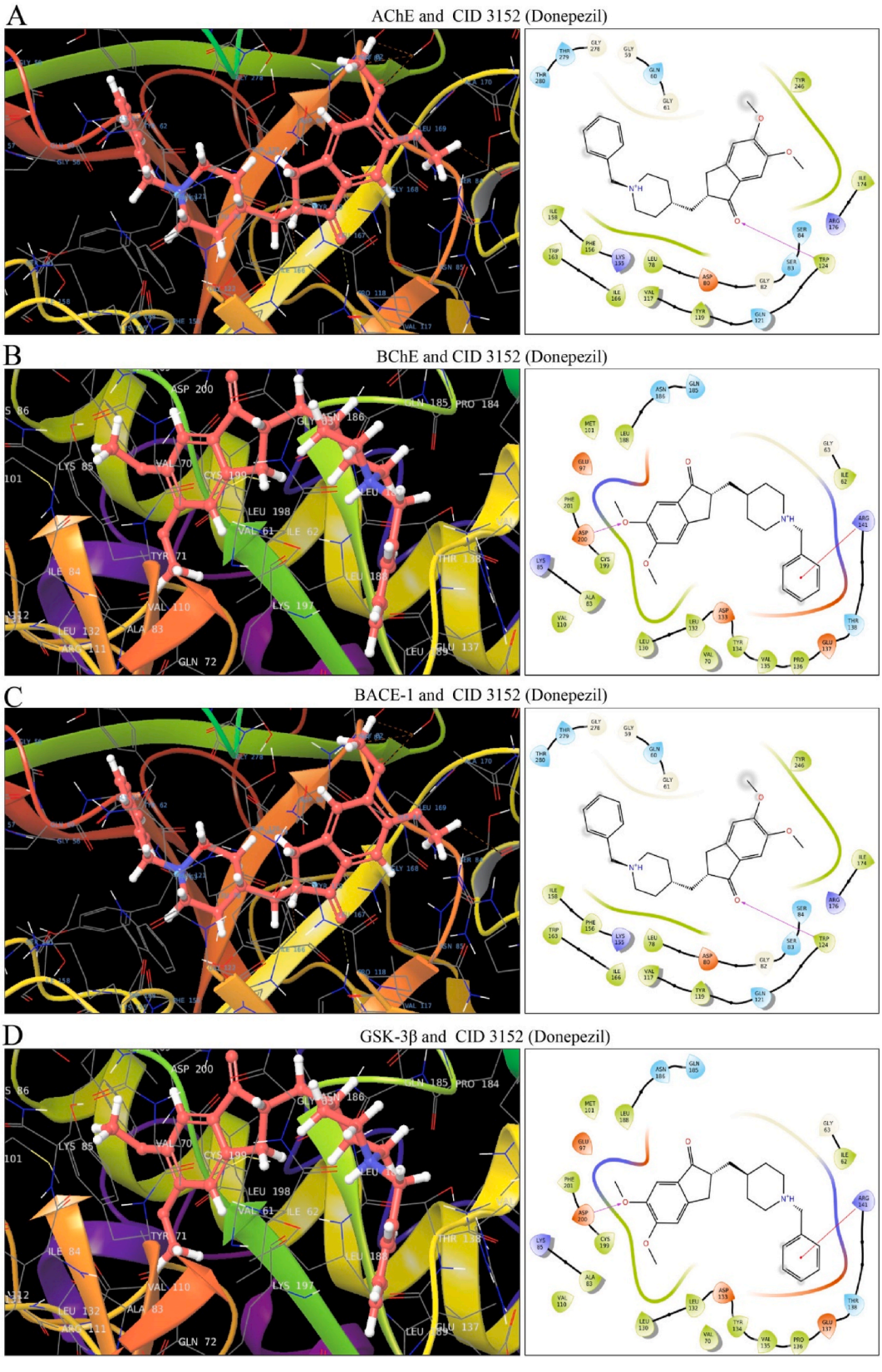

(caption on next page)

Fig. 5. Multi-modal molecular docking interaction of donepezil and neuronal pathologic targets. (A) AChE and CID 114943 (donepezil) (B) BChE and CID 114943 (donepezil), (C) BACE-1 and CID 114943 (donepezil), and (D) GSK-3β and CID 114943 (donepezil). Left side is 3D, right side is 2D of protein-ligand.

Table 2
Free energy of ligand binding to AChE, BChE, BACE-1 and GSK-3β obtained from post-docking MM-GBSA analysis.

Comp sounds	Target proteins	ΔG bind	ΔG bind coulomb	ΔG bind covalent	ΔG bind H-bond	ΔG bind lipo	ΔG bind packing	ΔG bind Solv GB	ΔG bind vdW
CID 114943 (Protober berine)	AChE	−67.652	−42.231	0.442	−0.212	−22.825	−9.545	46.163	−39.657
	BChE	−55.593	31.053	9.09E-13	−0.192	−19.877	−7.515	−23.639	−35.615
	BACE-1	−53.31	−25.422	0.453	−0.947	−17.081	−1.182	30.4	−30.478
	GSK-3β	−39.807	107.4037	0.341668	−0.692	−14.889	−0.57536	−99.3837	−32.704
CID 4970 (Protopine)	AChE	−45.386	−60.382	3.142	−0.09	−35.855	−5.413	99.879	−46.666
	BChE	−48.467	−5.236	0	−0.35	−26.948	−4.157	37.262	−49.038
	BACE-1	−48.081	−38.042	1.083	−0.098	−21.022	−1.919	52.845	−40.928
	GSK-3β	−32.89	36.42838	3.779758	−0.12758	−12.836	−0.17537	−23.3112	−36.647
CID 5284371 (Codeine)	AChE	−38.187	−52.878	3.664	−1.083	−31.569	−2.284	88.79	−42.826
	BChE	−49.244	−1.54	0	−0.871	−25.941	−3.182	22.056	−39.765
	BACE-1	−45.959	−46.431	7.431	−0.548	−22.804	−1.225	48.773	−31.155
	GSK-3β	−21.94	53.76659	3.316788	−0.79576	−16.856	−0.00888	−40.7078	−20.655
CID 3152 (Donepezil)	AChE	−65.634	−58.455	1.019	−0.225	−43.058	−7.847	91.212	−58.278
	BChE	−56.769	−1.98	0	−0.206	−32.18	−4.421	30.93	−48.912
	BACE-1	−51.264	−30.429	1.85	−0.848	−24.531	−1.555	50.044	−45.794
	GSK-3β	−41.375	46.21507	6.431545	−0.44476	−20.694	−0.10743	−31.7539	−41.021

All the energies are in kcal/mol. ΔG bind, ΔG bind coulomb, ΔG bind covalent, ΔG bind H-bond, ΔG bind lipo, ΔG bind Solv GB and ΔG bind vdW stands for binding energy, coulomb energy, covalent binding energy, energy due to H-bonds, lipophilic energy, solvation energy and van der Waal's energy, respectively.

Table 3
The designated phytochemicals' pharmacochemical, physical attributes, lipophilicity, solubility in water, drug-like characteristics, synthetic availability, and toxicity have been outlined in this table.

Properties		Protoberberine (CID 114943)	Protopine (CID 4970	Codeine (CID 5284371)	Donepezil (CID 3152)
Physico-chemical properties	MW (g/mol)	232.3	353.37	299.36	379.49
	Heavy atoms	18	26	22	28
	Aromatic. heavy atoms	16	12	6	12
	Rotatable bonds	0	0	1	6
	H-bond acceptors	0	6	4	4
	H-bond donors	0	0	1	0
Lipophilicity	Log Po/w(MLOGP)	3.5	1.9	1.98	3.06
Water solubility	Log S (ESOL)	−4.37	−4.13	−2.55	−4.81
Pharmacokinetics	GI absorption	High	High	High	High
	BBB permeation	Yes	Yes	Yes	Yes
Drug ability	Lipinski violation	0	0	0	0
Medicinal chemistry	Synthetic accessibility	2.42 (easy)	3.48 (easy)	4.89 (easy)	3.36 (easy)
Toxicity and mutagenicity	Hepatotoxicity	I	I	I	I
	Carcinogenicity	I	A	I	A
	Immunogenicity	I	A	I	A
	Cytotoxicity	I	I	I	A

Here, I mean Inactive and A means Active.

compound. The Log S scores for the three selected compounds and control drugs were −4.37, −4.13, −2.55, and −4.81, respectively. The analysis of water solubility revealed that all compounds were water-soluble according to the provided solubility scale. Additionally, all the screened compounds tested negative for hepatotoxicity. The exceptions were CID 4970 and CID 3152, which showed cytotoxicity and immunotoxicity. At the same time, CID 114943 and CID 5284371 found no toxicity profiling.

3.2.5. MD simulation analysis

The ligand-protein combination binding stabilization has been observed and measured by taking advantage of molecular dynamics (MD) simulations. During the coordination period, the MD simulation data was collected from interaction diagram and event analysis. During a 250 ns period, the stand ability of the protein-ligand was measured employing apo (only protein), three ligands (CID 114943, CID 4970, and CID 5284371), and the control medicine donepezil (CID 3152). The result was examined based on the protein-ligand

RMSD, protein RMSF, rGyr, hydrogen bonds, SASA, MolSA and protein-ligand contacts.

3.2.5.1. Protein root mean square deviation (RMSD) analysis. RMSD of a protein and ligand intricate structure helps determine the average distance a specific atom moves over a specified period in comparison with an appropriate time. The RMSD of the three chosen drugs and control was assessed for each AChE, BChE, BACE-1, and GSK-3β receptor to analyze alterations in protein structure in comparison from the beginning point. Protein equilibrium condition can also be established by flattening the RMSD curve. The simulation's lessened RMSD spectrum and steady shifts demonstrate that its protein backbone is stable. In contrast, a higher RMSD and significant divergence from the native structure indicate that the protein-ligand pair appears instability. A value exceeding the specified range signifies the protein underwent an enormous conformational alteration. It is perfectly permissible for an average or mean to deviate from a reference frame by a range of 1–3 Å. To evaluate the reliability of the protein's framework during a 250 ns simulation time, RMSD values of Cα atoms for the apoprotein selected three ligands protoberberine, protopine, Codeine, and donepezil protein-ligand complexes have been calculated and observed the alterations that are depicted in Fig. 6(A–C, E, & G) individually for AChE, BChE, BACE-1, and GSK-3β receptor when the three chosen ligands combined with the apoprotein, the RMSD of their intricate structure was compared with reference drugs. The highest, lowest, and average RMSD of each receptor are given in Table S14. For the AChE receptor, the apoprotein, the protoberberine, protopine, codeine complex, and the AChE-donepezil showed average RMSD values of 1.60 Å, 1.67 Å, 1.41 Å, 1.67 Å and 1.57 Å; whereas, the lowest to highest RMSD values were (0.85–2.024) Å, (0.85–2.09) Å, (0.8–0.781) Å, (0.95–2.14) Å, and (0.87–2.078) Å respectively as demonstrated in (Fig. 6A). As of BChE, the average Cα-RMSD, and lowest-highest RMSD values of the apoprotein, Lead complexes, and donepezil were 1.71 Å (1.08–2.14) Å, 1.91 Å (0.86–2.38) Å, 1.66 (0.96–1.99) Å, 1.48 (0.90–1.91) Å and 2.00 Å (1.15–2.45) Å correspondingly. Notably, none of these compounds showed significant variations during the study, remaining in an equilibrium state throughout the simulation (Fig. 6B). In the case of BACE-1, the average and lower-higher deviations of apoprotein 2.51 Å (1.03–4.58) Å and donepezil complex was 3.14 Å (1.20–5.08) Å whereas the three lead complexes calculated as of 2.78 Å (1.49–4.61) Å, 2.45 Å (1.22–3.64) Å, and 3.72 Å (1.01–5.35) Å which demonstrates no or low structural changes during the 250ns simulation (Fig. 6C). Similarly, for GSK 3β-protoberberine, protopine, and codeine complexes as depicted in the range was 1.19 Å to 3.21 Å, 1.03 Å to 3.13 Å, and 1.24 Å to 2.95 Å, whereas apoprotein and donepezil showed a range of 1.24 Å to 3.03 Å and 1.11 Å to 3.68 Å indicating good stability, resembling the selected compound as promising lead agents (Fig. 6D). All the complexes represented the approved ranges of average values less than 3 Å. Moreover, selected ligands-protein complexes showed less average fluctuation when equivalence with the donepezil control drugs and demonstrated almost similar fluctuations with apoprotein. This result depicted that the protoberberine, protopine, and codeine, when complexed with their respective receptor molecules, had le deviation.

3.2.5.2. Protein root mean square fluctuations (RMSF) analysis. Root Mean Square Fluctuation (RMSF) is used in computational biology and structural bioinformatics for assessing the flexibility and diversity of certain atoms or groups within a biomolecule over a while. It quantifies the extent to which atomic positions deviate from their average positions during simulations. The residues' RMSF value indicates the degree of stability and variation of protein of each amino acid in an intricate framework. A ligand may achieve enhanced stability if its amino acids have low RMSF values. The ligands and control drugs were designated with four receptors in particular, namely AChE, BChE, BACE-1, and GSK-3β, and the RMSF different aspects parameter were evidenced in Table S14. In AChE, apo-protein, three compounds, and control drugs allow the average fluctuation of 0.74 Å, 0.78 Å, 0.81 Å, 0.74 0.85 Å, and 0.87 Å, respectively. Whereas, the BChE showed the average values of 0.79, 0.85, 0.84, 0.78, and 0.91, correspondingly. As for BACE-1 and GSK-3β, the average values of 1.10 Å, 1.07 Å, 0.99 Å, 1.17 Å, 1.34 Å and 1.03 Å, 1.0 Å, 3.13 Å, 1.128 Å, 1.120 Å individually for each apo-protein, three lead compounds, and control drugs donepezil. The AChE, BChE, and BACE-1 convey the acceptable range of the average RMSF. Whereas GSK-3β demonstrates a slightly increased average value of 3.136 Å for protopine. Without these compounds, the other two compounds have acceptable ranged RMSF values. The RMSF values of AChE, BChE, BACE-1, and GSK-3β corroborate in Fig. 6 (E, F, G, and H). The Figure illustrated a few marked amino acids peaked at more than 3 Å and some higher peaks visualized at the start and end point due to the presence of N-terminal and C-terminal. In the Figure, the RMSF analysis observed regions of augmented flexibility, specifically, In AChE, GLY27, PRO344, ALA363, GLY415, and ASP494 residues, in BChE, GLY27, LEU76, GLY163, PRO344, LEU386, and ASP494 residues, in BACE-1, THR120, VAL214, ALA361, and HIS446, residues, and in GSK-3β, ASP58, LYS122, ASP192, GLY253, GLU290, and GLY353 residues respectively which are recognized for taking part in the binding of ligand. The less peaked RMSF values of AChE, BChE, and BACE-1 complexes indicate a trend of decreased atomic fluctuations in the biomolecule compared to the apo and control, whereas GSK-3β randomly fluctuated values indicated each receptor conformational bit instability.

3.2.5.3. Ligand root mean square deviation (RMSD) analysis. The ligand RMSD measures the overall structural stability by the ligand fluctuations or deviation from the active site of the respective protein. To determine the rigidity of selected compounds concerning control drugs, the ligand RMSDs of AChE, BChE, BACE-1, and GSK-3β were calculated in MD simulation illustrated in Fig. 7. The stable RMSDs fluctuate between 3 Å and the selected compounds ligand-RMSDs are in the suitable range. The highest, lowest, and average ligand RMSD of AChE, BChE, BACE-1, and GSK-3β, respectively, are depicted in Table S14. The protoberberine, protopine, codeine complex, and the AChE-donepezil showed average ligand RMSD values of 0.371 Å, 0.3 Å, 0.261 Å, and 0.575 Å; whereas, the lowest to highest ligand RMSD values were (0.11–0.55) Å, (0.12–0.65) Å, (0.80–0.68) Å, and (0.19–2.25) Å, respectively as demonstrated in (Fig. 7A). As of BChE, the average C-alpha of ligand RMSD, and lowest-highest RMSD values of the Lead complexes, and donepezil were 0.34 Å (0.06–0.62) Å, 0.24 Å (0.11–0.72) Å, 0.45 (0.12–0.70) Å, 1.74 Å (1.16–3.50) Å, correspondingly. During the simulation, it is

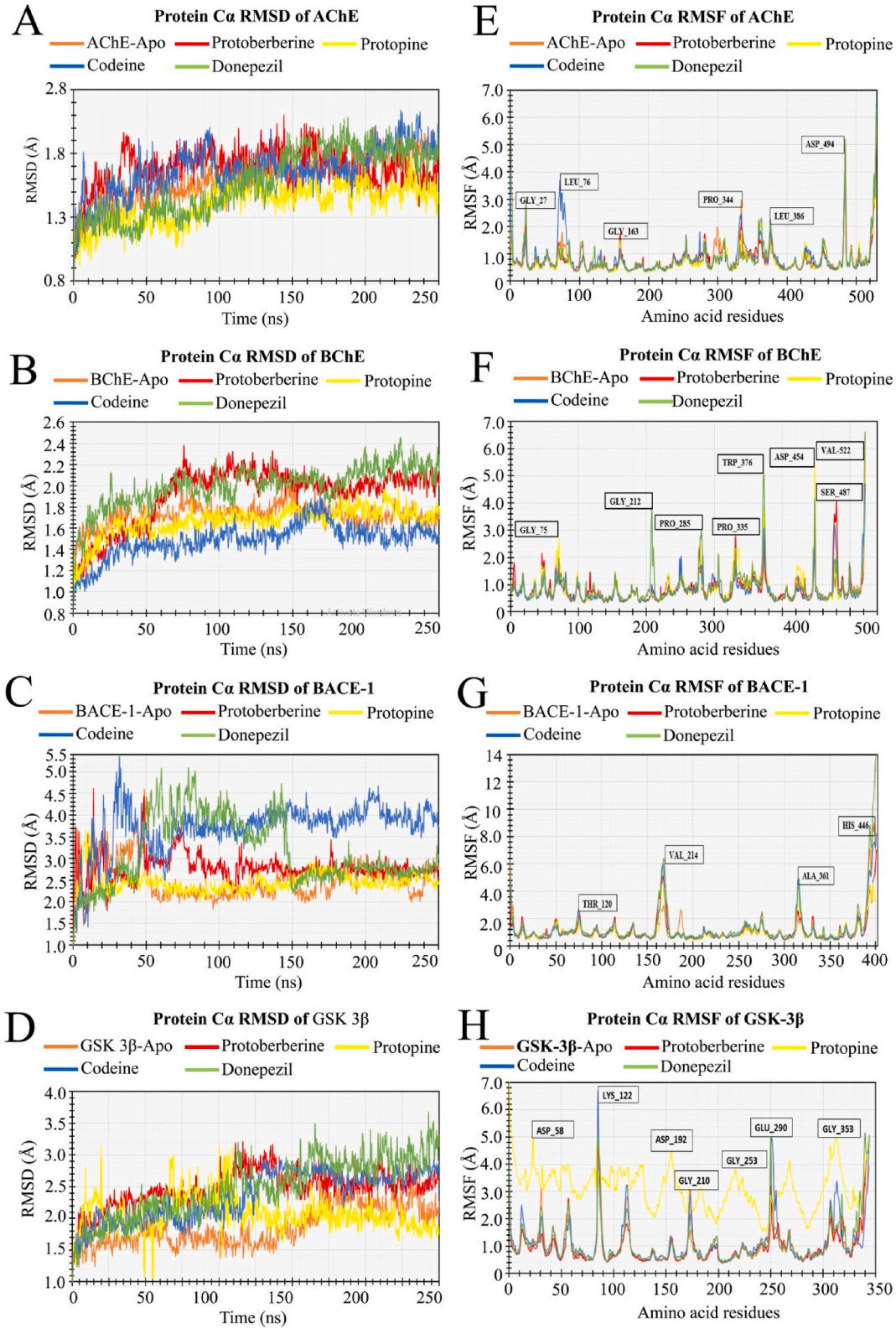

(caption on next page)

Fig. 6. Protein Cα RMSD and Cα RMSF values of the respective Apo protein (orange), protoberberine (red), protopine (yellow), codeine (blue) and donepezil (green) depicted at A, C, E, and G for AChE, BChE, BACE-1, and GSK-3β respectively. Whereas, B, D, F, & H illustrated the ligand Cα RMSD of protoberberine (red), protopine (yellow), codeine (blue), and donepezil (green) for AChE, BChE, BACE-1, and GSK-3β respectively in 250 ns simulation. (For interpretation of the references to color in this figure legend, the reader is referred to the Web version of this article.)

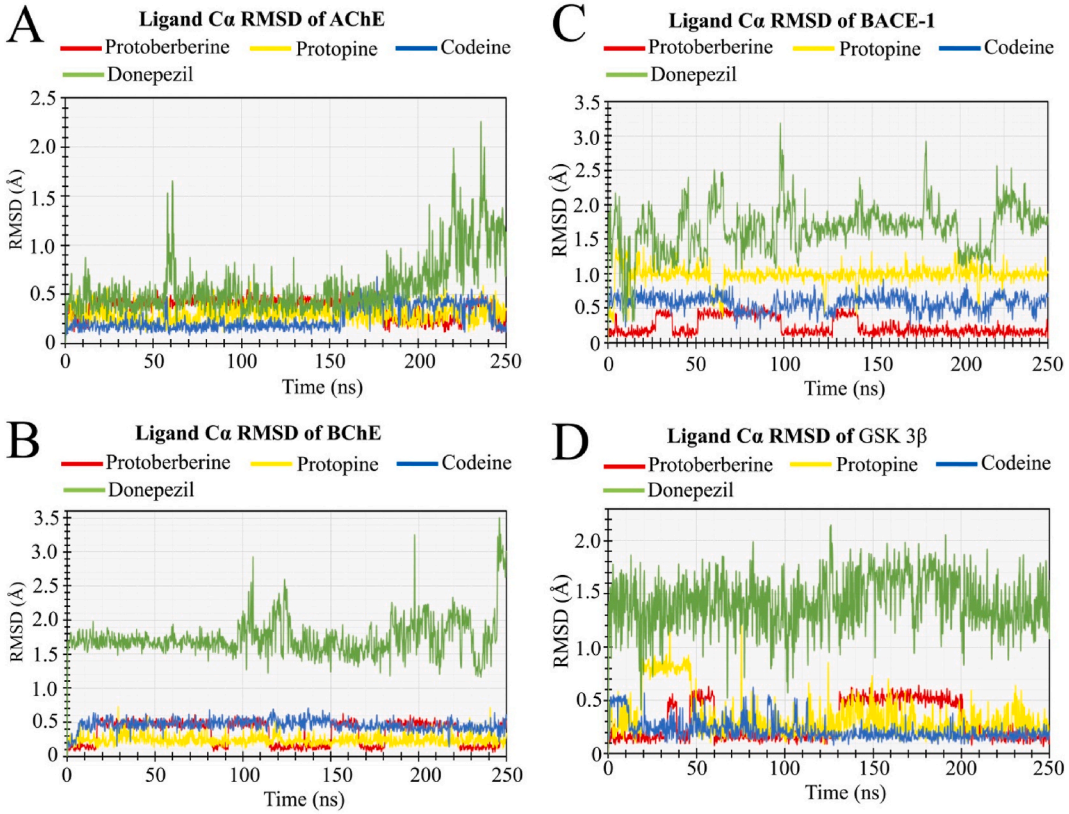

Fig. 7. The RMSD values obtained from the Cα atoms of the target protein-selected phytocompound docked complex were extracted. The complexes of AChE, BChE, BACE-1, and GSK-3β with protoberberine, protopine, codeine, and the control drug donepezil are denoted by the colors red, yellow, blue, and green, respectively. (For interpretation of the references to color in this figure legend, the reader is referred to the Web version of this article.)

noteworthy that none of these chemicals exhibited any notable fluctuations and remained stable (Fig. 7B). When it comes to BACE-1, the average and lower-higher deviations of the donepezil complex were 1.65 Å (0.31–3.175) Å; where, the three lead complexes calculated as of 0.23 Å (0.06–0.545) Å, 0.97 Å (0.29–1.50) Å, and 0.57 Å (0.19–0.92) Å which demonstrates no or low structural changes during the 250ns simulation (Fig. 7C). Additionally, the range of GSK 3β-protoberberine, protopine, and codeine complexes was 0.3 Å to 1.38 Å, 0.07 Å to 0.624 Å, and 0.419 Å to 2.14 Å, respectively. In contrast, donepezil exhibited a range of 0.07 Å to 0.64 Å, which suggests good stability and indicates the selected compound as a prospective candidate (Fig. 7D). In AChE, the control Donepezil drugs depicted higher peaks after the 180ns simulation time frame, whereas the lead compounds' fluctuation was minimal. Similarly, BChE, BACE-1, and GSK-3β visualized the maximal fluctuation at donepezil. The lead compounds protoberberine, protopine, and codeine calculated very lower fluctuation from the protein binding site, indicating that these three compounds have structural durability when bound with respective proteins.

3.2.5.4. Radius of gyration analysis. A protein's accessibility and firmness can be measured by assessing the organization of atomic particles along its direction, which is referred to be the radius of gyration (rGyr) in protein-ligand multifaceted structures. It also provides structural rigidity, indicating the compactness and the folding or unfolding of the protein molecules. Wherefore, Protoberberine (CID 114943), protopine (CID 4970), codeine (CID 5284371), and control drug donepezil (CID 3152) with the respective protein of AChE, BChE, BACE-1, and GSK-3β protein-ligand complexes stability was analyzed in respect to rGyr over 250 ns exhibited at Fig. 8. A root-mean-square radius from the atomic centers of mass was computed for each complex and all the macromolecules exhibited less average fluctuations in contrast with the donepezil control drug that illustrated in Table S15. The lead compounds (protoberberine, protopine, and codeine) in complex with AChE, BChE, BACE-1, and GSK-3β receptors showed average rGyr values of (3.22 Å, 3.94 Å, and 2.98 Å) for AChE; (3.22 Å, 3.86 Å, and 3.00 Å) for BChE; (3.22 Å, 3.76 Å, and 3.00 Å) for BACE-1; (3.22 Å, 3.87 Å,

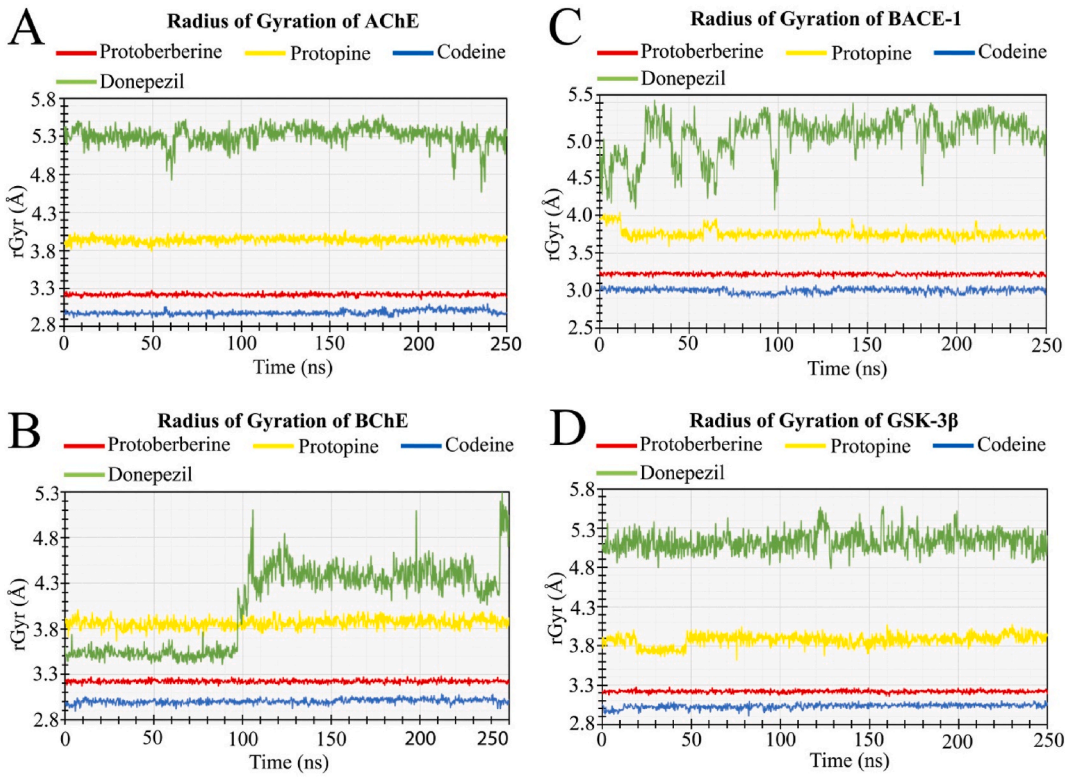

Fig. 8. The radius of gyration (rGyr) of the target protein-phytocompound complexes was measured. The rGyr values of the selected phytocompounds protoberberine, protopine, and codeine and the control drug, donepezil, in complex with AChE, BChE, BACE-1, and GSK-3β are denoted by red, yellow, blue, and green colors, respectively, during a 250 ns simulation. (For interpretation of the references to color in this figure legend, the reader is referred to the Web version of this article.)

3.03 Å) for GSK-3β, respectively. While the control drug donepezil average rGyr values of 5.31 Å, 4.05 Å, 5.06 Å, and 5.12 Å, respectively for the selected four receptors. The selected ligands have adequate average values with short lengths of higher and lower fluctuation distances for the four nominated receptors. This admissible rGyr analysis confirmed the less conformational instability when ligands bind with its receptor protein of AChE, BChE, BACE-1, and GSK-3β active site.

3.2.5.5. Solvent accessible surface area (SASA) analysis. SASA is a computational method constructed to comprehend the biomolecules' molecular makeup and function as well as to measure a biomolecule's exposed surface area that is accessible to molecular solvents. The outermost residues of structures usually serve as binding sites through which they interact with drugs as well as additional molecules. SASA analysis facilitates identifying a complex's solvent-like actions, whether it attracts water or not. In this study, SASA values of each receptor (AChE, BChE, BACE1, and GSK-3β) when complexed with ligands demonstrated much similar values, and some complexes estimated better result than the donepezil that illustrated in Fig. 9A–C, E and G. Both the complexes showed a stable profile from the beginning of the simulation to the last time of the 250 ns simulation time frame, as evidenced in Table S16. The AChE and BChE protein when complexed with the protoberberine, protopine, codeine, and control drug, exhibited the average SASA values of 25.68 $Å^2$, 17.19 $Å^2$, 39.44 $Å^2$, 70.61 $Å^2$ and 149.11 $Å^2$, 62.06 $Å^2$, 77.19 $Å^2$, 45.02 $Å^2$, respectively. While the BACE-1 and GSK-3β calculated the average values of 94.72 $Å^2$, 103.56 $Å^2$, 20.73 $Å^2$, 213.49 $Å^2$, and 50.68 $Å^2$, 352.19 $Å^2$, 74.55 $Å^2$, 175.26 $Å^2$ for the three lead and control drugs. The table shows that all three receptors' protein and protein-ligand complexes have appreciable nonpolar-polar interactions.

3.2.5.6. Molecular surface area (MolSA) analysis. MolSA is a measurement of the size and shape of a ligand and protein when it is in complex formation. It also predicts the binding interaction of ligand-protein complexes. In MDS, MolSA determines each atom's location and particular acceleration within a complex in a specific time manner that accesses the dynamic manner of the complexes. Here, the AChE, BChE, BACE-1, and GSK-3β in combined with Protoberberine (CID 114943), protopine (CID 4970), codeine (CID-5284371), and control drug donepezil (CID 3152) 250 ns time frame of MolSA is evaluated. The molSA of every complex showed some random fluctuations initially. However, after time, it increased and observed very well-mannered molSA values over the last simulation in comparison with the donepezil drug that is ascertained in Fig. 9B–D, F and H. A larger MolSA indicated that the ligand-protein complexes needed more surface, indicating that the complex is more flexible. The MolSA values of each receptor denoted the wide range of acceptable values depicted in Table S16. The protopine (CID 4970) showed the average values with all selected receptor

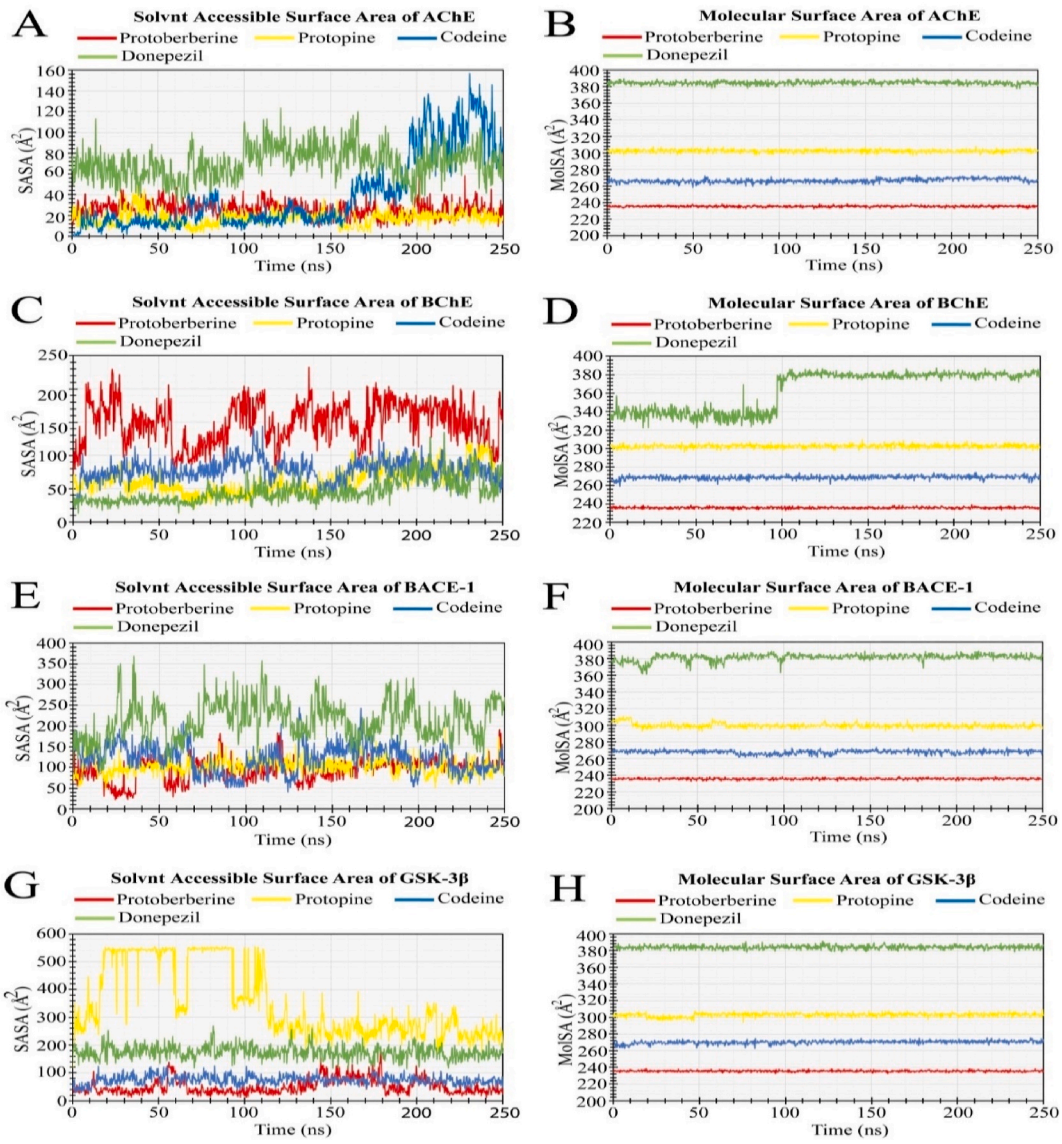

Fig. 9. Solvent accessible surface area (left side) and molecular surface area (right side) representative ligands and AChE, BChE, BACE-1, and GSK-3β complexes calculated from a 250-ns simulation. (A, C, E, and G) SASA analysis, and (B, D, F, and H) MolSA analysis.

molecules, which are 302.381 Å^2, 302.599 Å^2, 299.739 Å^2, and 303. 012 Å^2 where the control drug donepezil has the average MolSA of 384.735 Å^2, 363.071 Å^2, 381.437 Å^2, and 383.917 Å^2 for the AChE, BChE, BACE-1, and GSK-3β respectively. The other compounds of protoberberine (CID 114943) and codeine (CID 5284379) with AChE, BChE, BACE-1, and GSK-3β exhibits the average values of 235.651 Å^2 & 266.743 Å^2, 235.739 Å^2 & 268.612 Å^2, 235.810 Å^2 & 268.009 Å^2, and 235.735 Å^2 & 270.139 Å^2 respectively.

3.2.5.7. Hydrogen bond analysis. Hydrogen bonds are the strongest noncovalent bonds, other kinds of bonds when ligands bind with protein. A new drug molecule's specific binding in the inhibitory site depends on the essential hydrogen bonds. Drug specificity, metabolism, and adsorption are all influenced by hydrogen bonds at a drug-binding site, which is crucial to the interaction between the drug and the targeted protein. With AChE, BChE, BACE-1, and GSK-3β proteins, several bonds of hydrogen analyzed for the chosen compounds of protoberberine, protopine, codeine, and donepezil control drug have been indicated in Fig. 10. The bond strength of hydrogen was obtained for each specified complex during the 250 ns simulation, from the start of the simulation to conclude. In all the complexes, the hydrogen bonds range between 320 and 516 simultaneously in a 250 ns time frame, as demonstrated in Table S15. The selected compounds with the respective protein molecules exhibited acceptable numbers of hydrogen bonds when compared with control drug molecules.

3.2.5.8. Protein-ligand contact analysis. Interactions of proteins with the designated three of substances, including protoberberine,

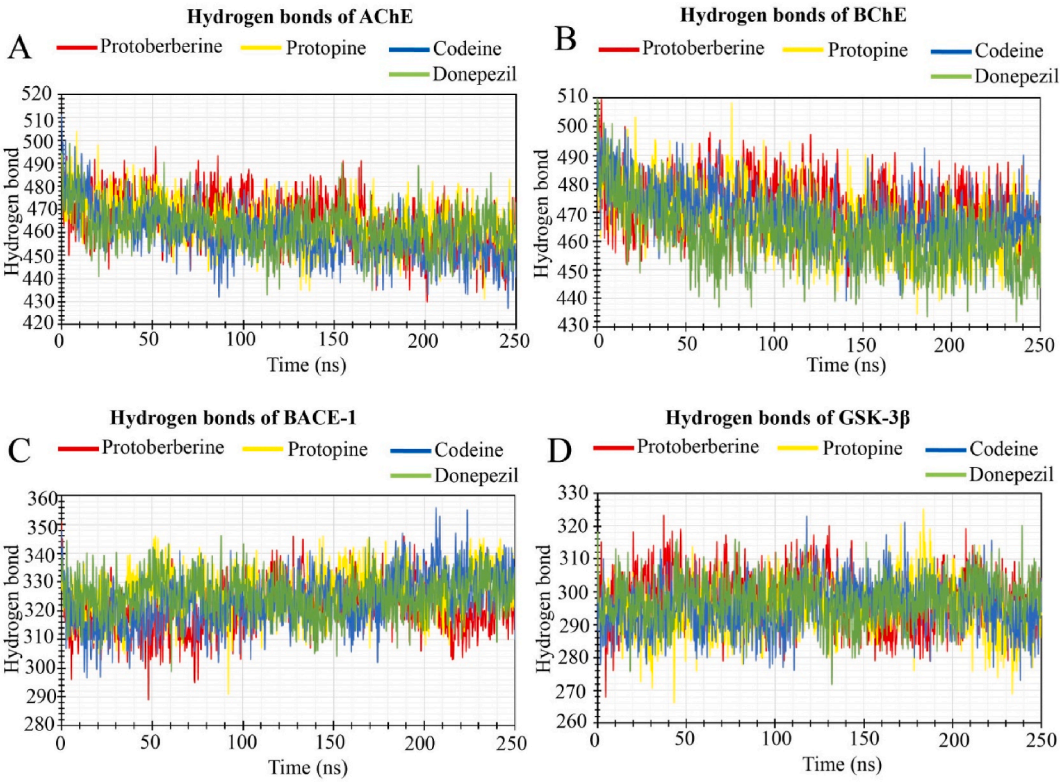

Fig. 10. Hydrogen bonding calculation of the representative ligands complexes from a 250-ns simulation. Here, (A) Hydrogen bonds of AChE, (B) Hydrogen bonds of BChE, (C) Hydrogen bonds of BACE-1, and (D) Hydrogen bonds of GSK-3.

protopine, and codeine, along with the donepezil for each receptor of AChE, BChE, BACE-1, and GSK-3β have been observed from the 250 ns simulation time. The stacked bar charts in Figs. S7, S8, S9, and S10 depict the hydrogen bonds and hydrophobic, ionic, and water bridge bonding. Upon completion of the simulation, it was found that every compound underwent numerous interactions that concluded that the ligands had bonded in the protein's active region. Hydrogen and hydrophobic bonds are the key regulatory bonds for the protein-ligand binding stability for a long period. The stacked bar charts for protoberberine are shown in Fig. S7, with an interaction fraction value (IFV) of a maximum of 1.55 (TRP 86) and 1.8 (TYR 337) for AChE; 0.5 (ASP70) and 1.4 (TYR332) for BChE; 0.55 (TYR119) and 0.6 (PHE156) for BACE-1; 0.5 (ALA83)and 0.6 (LEU188) for GSK-3β, respectively at the residue TYR341 and TRP86, TRP82 and TYR119 which makes contact by using different type of hydrophobic ionic and water bridge For the protopine compounds shown in Fig. S8, the IFV found a maximum of 1.2 (HIS447) that has formed by hydrophobic, ionic, and water bridge bonds indicating 175 % interaction with AChE. IFV also found 1.0 at PHE338 produced by hydrophobic, ionic, and water bridge bond and 1.00, 0.98, and 0.75 at TRP86, TYR337 and PHE297 both are produced by hydrophobic, hydrophobic, and hydrophobic-water bridge bond maintaining 100 %, 98 % and 75 % interaction with AChE. While TRP82 (1.0), PHE329 (0.6), and TYR332 (0.6) with BChE, ASP80 (0.6), TYR119 (1.2), and PHE156 (0.8) with BACE-1 and TYR117 (0.6) with GSK-3β protein respectively during the simulation time. Another lead compound codeine depicted in Fig. S9, the IFV was calculated at the position of TRP86 (0.98), GLY121 (0.7), GLU202 (0.7), TYR337 (0.95) for AChE, TRP82 (0.98), GLY116 (0.5), PHE329 (0.55), TYR332 (0.8), HIS438 (0.5) for BChE, GLY59 (0.4), ASP80 (0.30), TRP163 (0.3) FOR BACE-1 and VAL70 (0.6), ASP200 (1.75) with GSK-3β protein respectively during the simulation time. Whereas the control ligand donepezil (CID 3152) demonstrated in Fig. S10, it has found to form multiple interactions at the position of TRP86 (1.75), TYR341 (1.0) for AChE, PHE329 (1.2) and TYR332 (0.85) for BChE, TYR119 (0.35), GLN121 (0.3) for BACE-1, and ASN64 (1.5), and GLU97 (1.75) for GSK-3β, the specific interaction is maintained and helped to make a stable binding with the desired protein. This interaction denoted that the selected compound has potential in AChE, BChE, BACE-1, and GSK-3β structures.

3.3. In vitro biological activity

3.3.1. In-vitro antioxidant activity of MEAMLF, EEAMLF, and EAEAMLF

Free radicals, which have unpaired electrons, are highly reactive and can be produced in various ways, such as regular metabolic activity, pollutants, and radiation. They cause oxidative stress in cells, DNA, and proteins, and are connected with numerous diseases including inflammation, cancer, neurodegenerative diseases, aging, and many multifactorial diseases [30]. Therefore, the production of free radicals must be eliminated, and compensation through dietary supplements, nutraceuticals, or plant-based phytochemicals is promptly needed. In this study, MEAMLF, EEAMLF, and EAEAMLF scavenged DPPH and H_2O_2 free radicals

concentration-dependently. In the DPPH assay, MEAMLF, EEAMLF, and EEAMLF showed inhibition ranging from 11.9135 % to 84.43714 %, 14.34678 %–86.7775 %, and 10.76325 %–79.6816 %, respectively, whereas the IC_{50} values were 4.589 μg/mL, 4.380 μg/mL, and 4.837 μg/mL, respectively showed in Fig. 11 A. In the H_2O_2 assay, ascorbic acid, MEAMLF, EEAMLF, and EAEAMLF showed inhibition ranging from 29.48696 % to 95.29159 %, 11.75445 %–82.51547 %, 10.91369 %–79.58502 %, and 9.8647 %–77.54356 %, correspondingly, while the IC_{50} values were 2.593 μg/mL, 4.146 μg/mL, 4.371 μg/mL, and 4.575 μg/mL, respectively, as depicted in Fig. 11 B. Both assays yielded promising results compared to the standard drug ascorbic acid, with acceptable ranges of IC_{50} values. The DPPH method showed better scavenging than the H_2O_2 method. In the DPPH method, the methanol extract showed higher inhibition, whereas in the H_2O_2 method, ethanol extracts depicted higher inhibition.

3.3.2. Acetylcholinesterase and butyrylcholinesterase inhibition activity

Acetylcholinesterase and butyrylcholinesterase are the predominant enzyme accountable for the process by which the neurotransmitter acetylcholine and butyrylcholine are degraded. Therefore, it is imperative to invent therapeutic agents that can cure AD by inhibiting the AChE and BChE enzyme. The assessment of AChE and BChE inhibitory potential of MEAMLF, EEAMLF, and EAEAMLF was conducted to determine the prospect of therapy of the *Argemone mexicana* plant. For AChE inhibition, the respective extracts of the MEAMLF, EEAMLF, and EEAMLF demonstrated an inhibition extending from 23.507 % to 56.527 %, 25.729 %–60.173 %, and 17.569 %–52.083 %, correspondingly with IC50 values of 5.77 μg/mL, 5.25 μg/mL, and 6.61 μg/mL, accordingly that depicted at Fig. 12A. Whereas, for the BChE inhibition, the MEAMLF showed 17.322 %–58.743 %, the EEAMLF denoted 20.596 %–61.297 % and EEAMLF illustrated an inhibition ranging from 18.337 % to 54.617 %, respectively, with relative IC_{50} values of 6.50 μg/mL, 6.120 μg/mL, and 6.852 μg/mL, respectively as shown in Fig. 12 B. Donepezil was utilized as a standard drug, exhibiting an inhibition ranging from 29.805 % to 73.26 % with IC50 values of 4.049 μg/mL for AChE inhibition and 27.57 %–73.15 % inhibition with IC_{50} calculation of 5.164 μg/mL BChE. The EEAMLF extract showed considerably better results compared to the MEAMLF and EEAMLF for both AChE and BChE inhibition. The results indicate that *Argemone Mexicana* contains phytoconstituents that have a favorable inhibitory and binding affinity with the AChE and BChE active site.

4. Discussion

Alzheimer's disease is a developing, multifaceted neurological disorder. Currently, no effective treatment to cure this disease, and existing treatments only target the cholinergic pathway, providing symptomatic relief rather than the cure of the disease. The concept of 'one disease, one target, 'one medication' cannot address the complexities of neurodegenerative diseases. These constraints have led us to investigate creating innovative therapies that utilize multiple targeted methods to address several different pathological processes of Alzheimer's disease at the same time.

Recently there is increasing interest in in investigating plant-derived phytochemicals because of their diverse biological function and structures with no or low side effects [28]. Therefore, we centered on investigating the anti-AD prospective of *Argemone mexicana* leaf and flower extracts, as well as their phytocompounds. While previous research has explored the antioxidant, anti-inflammatory [32], antianxiety [33], antidiabetic, and neuroprotective effects [34] of these plant extracts against cerebral ischemia-reperfusion injury, there is insufficient information about their action against Alzheimer's disease and the specific phytocompounds of this plant. In this study, we focused on investigating the anti-Alzheimer's disease potential of *Argemone mexicana* leaf and flower extracts, as well as their phytocompounds that have multi-targeting ability against multiple factors of Alzheimer's disease, such as AChE, BChE, BACE-1, and GSK-3β.

To utilize phytocompounds metabolically annotated by GC-MS from *Argemone mexicana* leaf and flower extracts in drug discovery,

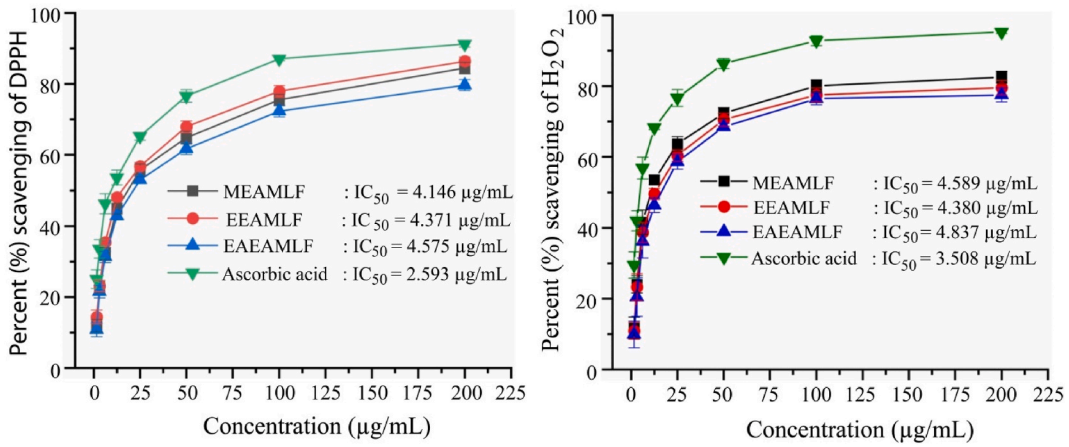

Fig. 11. *In vitro antioxidant* activities of different extracts of leaves and flowers of *Argemone mexicana* at various concentrations. (A) DPPH radical scavenging activity. (B) Hydrogen peroxide (H_2O_2) radical scavenging activity. Each value represents a mean ± STDEV of three separate experiments. MEAM = methanol extract, EEAM = ethanol extract, and EAEAM = ethyl acetate of *Argemone mexicana* leaves and flowers.

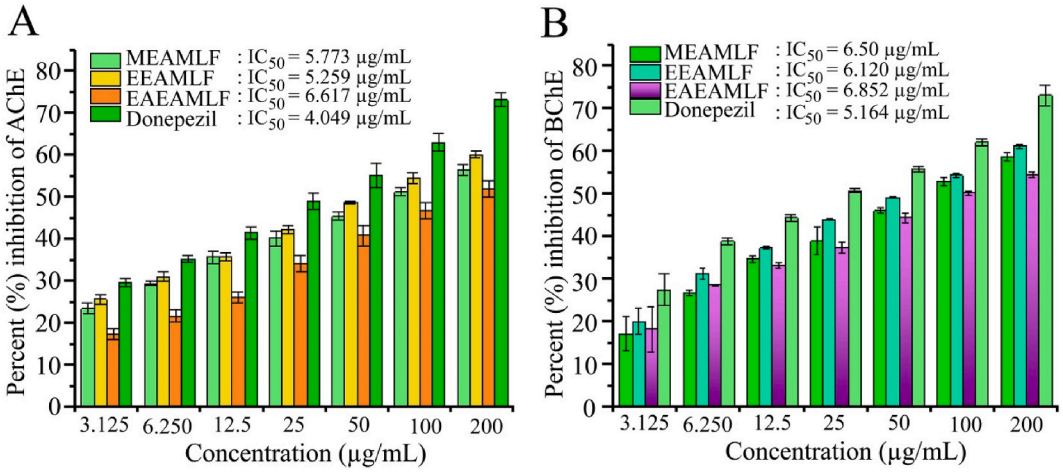

Fig. 12. *In vitro* acetylcholinesterase (AChE) and butyrylcholinesterase (BChE) inhibitory activity of *Argemone mexicana* leaves and flowers extracts. (A) Anti-acetylcholinesterase activity. (B) *Anti*-butyrylcholinesterase activity. Each value represents the mean ± standard deviation (STDEV) of three separate experiments performed at each concentration of the extracts.

in silico study is essential due to its speed and cost-efficiency compared to traditional *in vitro* methods [35]. In the first step of molecular docking simulation of an *in silico* study, three promising phytochemicals (protoberberine, protopine, and codeine) exhibited multi-targeting ability with better binding affinity to AChE, BChE, BACE-1, and GSK-3β compared to control drug donepezil. In accordance with our results, a natural product, notopterol from *Notopterygium incisum*, showed dual inhibitory activity against BACE-1 and GSK-3β [36]. This suggests that developing a multi-target-directed ligand may be an effective therapeutic strategy. Density function calculation is another important analysis that helps to predict the pharmacological character, understanding the chemical reactivity and kinetics stability of ligand molecules. Previously, A. Samad et al. suggested that the greater energy gap denotes the reactive compounds while the less energy gap signifies the hit compounds energetically favorable [37]. In our case, the three lead ligands calculated favorable gap energy, hardness and softness values rather than the control drugs (Table S12). Next, our post-docking MM-GBSA analysis, which is an accurate method to evaluate protein-ligand stability in the presence of a solvent, supported our compound evaluation to select the best drug candidates. Through MM-GBSA analysis, protoberberine, protopine, and codeine were identified as the most efficacious hits based on their superior negative binding affinity and binding free energy towards AChE, BChE, BACE-1, and GSK-3β compared to the control drug donepezil. In agreement with our findings, Danish Iqbal et al. (2021) reported that the MM/GBSA study demonstrated the formation of a stable protein-ligand complex between the natural compound (3-(2-methoxyphenyl)-4-oxo-4H-chromen-7-yl 4-methylbenzoate) and both AChE and BChE. In the subsequent phase of our *in silico* study, each of the three hit compounds had a molecular mass under 500 g/mol, demonstrated high gastrointestinal absorption, did not violate Lipinski's rule, and were deemed suitable for BBB permeation with no toxicity. Additionally, these hit compounds exhibited favorable physicochemical properties, such as lipophilicity, water permeability, and synthetic accessibility. These attributes make these three hit compounds appealing candidates for anti-AD therapeutics, prompting their selection for further molecular dynamics simulation (MDS) studies. The MDS analysis revealed that protoberberine, protopine, and codeine had stable interactions with AChE, BChE, BACE-1, and GSK-3β, as evidenced by the analysis of RMSD, RMSF, rGyr, SASA, MolSA, protein-ligand contacts (Figs. S6, S7, S8, and S9) and simulation snapshots (Fig. S11), affirming their potential as effective anti-AD lead phytochemicals. Correspondingly, in our results, Danish Iqbal et al. (2021) also performed MD simulations of the complex of the natural compound 3-(2-methoxyphenyl)-4-oxo-4H-chromen-7-yl 4-methylbenzoate with the targets AChE, BChE, MAO-A, and MAO-B. They found that the natural compound remained inside the binding cavity of the targets in a stable conformation throughout the MD simulation. The RMSD values calculated the stability of the protein-ligand complexes whereas the RMSF values denoted the structural flexibility of each residues presented in the selected macromolecules. The carbon alpha (Cα) atoms are the important parameters for MD simulation. The lower range of Cα values in RMSD and RMSF analysis the higher levels of the stability and flexibility. In this study, all the complexes provided the acceptable range of RMSD and RMSF results that confirms the three lead compounds when complexed with respective AChE, BChE, BACE-1, and GSK-3β confirms the stable binding of their active pocket cavity. A downward rGyr values designates the better compactness of protein-ligand complexes, while an upward rGyr values indicates the disassociation of ligands from the protein. The selected three ligands demonstrated least rGyr peaks than the control drug Donepezil, that indicates that the lead compounds binds with protein with more compactness. A larger MolSA and SASA values indicates less stable complexes where the lower values signifies the ligand tightly attached with protein amino acid residues. The selected three compounds showed higher stability in MolSA and SASA analysis parameters those play crucial roles in drug discovery process. The hydrogen bond analysis revealed critical interactions stabilizing the protein-phytochemicals complex, elucidating the best binding modes. Simultaneously, the analysis of protein-phytochemicals contacts emphasized specific residues crucial for binding affinity. Protein-ligand contacts analysis suggesting the specific protein residues, which interacted in a dynamics motions in MD simulation analysis. It also measures the strength of interaction in the active site. In this study, the three hit compounds and control drug demonstrated multiple common interacting

residues that denoted that the ligand binds in the protein active site.

Protoberberine is a natural plant-based alkaloid. In consistent with our result, research reports have suggested that protoberberine is also found in several species such as *Berberis vulgaris* L., *Berberis aristata* DC., *Berberis crataegina* DC., *Mahonia aquifolium* (Pursh) Nutt., *Hydrastis canadensis* L., *Xanthorhiza simplicissima*, *Coptis chinensis* Franch., *Tinospora cordifolia* (Thunb.) Miers (Giloy) and *Eschscholzia californica* Cham. Although not directly, but indirectly, aligns with our result that protoberberines has been reported to exhibit neuroprotective role in the context of antioxidant, anticonvulsant, and cerebral ischemic disorder properties [38]. Our results correspond with studies indicating that berberine, classified as a type of protoberberine, diminishes Aβ generation and lower the production of the β-site APP cleaving enzyme (BACE-1) via stimulating AMPK in mouse neuroblastoma cells N2a and primary cultured cortical neurons [39]. Moreover, protoberberine also exhibits various biological activities such as hypotensive, pain reliever, anti-amnesia, narcotic, antiarrhythmic, and antihemorrhagic, anti-inflammatory, antitumoral, antidiarrhetic, and antiulcer [40].

Another promising lead phytochemical, protopine was annotated both in methanol and ethanol extract in our study. Similar to our findings, other several research studies detected the presence of protopine in *Macleaya cordata* (Willd.) R. Br., *Dactylicapnos scandens* (D. Don) Hutch. and *Fumaria schleicheri* Soy.-Will. This compound has been reported to have a broad spectrum of pharmacological activates such as anti-inflammatory [41], anti-cancer [42], down regulation of glutamate levels in the brain, and decrease of intracellular calcium [43]. In addition, studies conducted in living organisms support the potential of this alkaloid to combat neurodegenerative disorders. Protopine has been shown to improve memory in mice with scopolamine-induced amnesia and enhance learning capacity in normal rats [44]. It also exhibits anticonvulsant activity in albino mice [45] and antidepressant activity in BALB/cj mice [46].

Our third lead phytochemical codeine is also an alkaloid-type phytochemical. Consistent with our study, codeine is detected in opium poppy, *Papaver somniferum* L., in addition to *Argemone mexicana* [47]. However, it is alkaloidal opioid-type established drug that acts on the opioid receptors in the brain. Codeine is commonly employed in prolonged pain management among individuals with Parkinson's disease [48] and psychiatric issues like feeling anxious or depressed [49].

However, multi-target potential of protoberberine, protopine, and codeine supported our initiative to conduct *in vitro* experimentation of *Argemone mexicana* leaves and flower extracts to elucidate their activity in AD. The pathology of cholinergic pathway include disruption of cholinergic activity driven by the enzymes AChE and BChE and AChE's and BChE's over activation also influences the overproduction and accumulation of Aβ. Our anti-AChE and BChE inhibition assay resulted that concentration dependent AChE and BChE inhibitory activity indicating that these extracts contain bioactive phytochemicals like protoberberine, protopine, and codeine that exhibit anti-cholinesterase activity.

The pathology of oxidative stress pathway drive the generation of reactive oxygen species (ROS) are closely linked to AD through a vicious cycle of triggering AGEs, interacting AGEs to RAGEs activating NF-kB, and NF-kB activation upregulates BACE-1 and GSK-3β, which induces phosphorylation of Tau (P-Tau), influencing the expression of AChE, which interacts with PS-1 to overproduce Aβ. Therefore, we conducted antioxidant activity of the extracts by scavenging DPPH and H_2O_2 to showcase the effect of this plant on AD. Our result showed the dose-dependent antioxidant activity indicates extract contains bioactive phytochemicals thereby supporting our *in silico* result.

The identified three lead phytochemicals are alkaloids and from previous research supports that alkaloids compounds have higher antioxidant activity that scavenge the ROS and help to treat neurodegenerative disease [50]. Scientist communities have yet to report no studies as these lead compounds' multi-targeted action against Alzheimer's disease. Moreover, these lead compounds have multifaceted uses that can suggest drug repurposing. Extensive wet-lab-based experimental research work is necessary on model organisms and Alzheimer's patients to ensure these compounds' appropriate efficacy and effect.

5. Conclusions

Through in silco study, we concluded that protoberberine (CID 114943), protopine (CID 4970), and codeine (CID 5284371) are the lead compounds showed the best binding affinity against all the four targets and exhibited the finest drug likeness and physicochemical properties which can cross the BBB as well as high absorption through GI tract with non-toxic potential. The findings of this study suggest that the protoberberine, protopine, and codeine can be a potential candidate against multiple-targets of three pathophysiological pathways like cholinergic, amyloidogenic, and neurofibrillary tangle pathways pertaining to AD. These findings are supported by the presence of these phytochemicals in the extracts of the leaves and flowers of the *Argemone mexicana* L. plant, as the extracts inhibited the activity of AChE and BChE, key proteins in the cholinergic pathway. The extracts also exhibited antioxidant activity by scavenging ROS, which provide pivotal neuronal signals that can lead to the over activation of AChE, BChE, BACE-1, and GSK-3β, resulting in Aβ accumulation and Tau phosphorylation. In this study, the neuroprotective potential of the candidate drug was explored through multi-target directed *in silico* approaches and *in vitro* experiments, aiming to combat Alzheimer's disease. This opens the door for confirmation of its therapeutic efficacy through full in vivo systems.

Ethical considerations

No ethical consideration has been involved in the research.

Funding

This work is financially supported by the grant (Grant no. SRG-231214) from the Ministry of Science and Technology (MOST) of the

People's Republic of Bangladesh and the Research Cell at Jashore University of Science and Technology in Bangladesh, under Grant ID JUST/Research Cell/22-FoBST-06/2023–2024.

CRediT authorship contribution statement

Md. Enamul Kabir Talukder: Formal analysis, Investigation, Methodology, Writing – original draft. **Shahina Akhter:** Conceptualization, Validation, Writing – review & editing. **Foysal Ahammad:** Resources, Software, Writing – review & editing. **Asmim Aktar:** Formal analysis, Investigation, Methodology. **Md. Saidul Islam:** Conceptualization, Writing – review & editing. **Aysha Akter Laboni:** Formal analysis, Methodology. **Mirola Afroze:** Formal analysis, Methodology. **Mala Khan:** Formal analysis, Methodology. **Mohammad Jashim Uddin:** Conceptualization, Funding acquisition, Writing – review & editing. **Md. Mashiar Rahman:** Conceptualization, Funding acquisition, Resources, Visualization, Writing – review & editing.

Declaration of competing interest

The authors declare that they have no known competing financial interests or personal relationships that could have influenced the work presented in this paper.

Acknowledgements

The authors extend their appreciation to the Laboratory of Computational Biology, Biological Solution Centre, Jashore, Bangladesh for supporting molecular docking and dynamic simulation.

Appendix A. Supplementary data

Supplementary data to this article can be found online at https://doi.org/10.1016/j.heliyon.2024.e37178.

References

[1] T. Kunkeaw, U. Suttisansanee, D. Trachootham, J. Karinchai, B. Chantong, S. Potikanond, W. Inthachat, P. Pitchakarn, P. Temviriyanukul, Diplazium esculentum (Retz.) Sw. reduces BACE-1 activities and amyloid peptides accumulation in Drosophila models of Alzheimer's disease, Sci. Rep. 11 (2021) 1–11, https://doi.org/10.1038/s41598-021-03142-w.
[2] X. Du, X. Wang, M. Geng, Alzheimer's disease hypothesis and related therapies, Transl. Neurodegener. 7 (2018) 1–7, https://doi.org/10.1186/s40035-018-0107-y.
[3] Q. yue Xiao, T. yuan Ye, X. long Wang, L. Han, T. xing Wang, D. mei Qi, X. rui Cheng, S. qi Wang, A network pharmacology-based study on key pharmacological pathways and targets of Qi Fu Yin acting on Alzheimer's disease, Exp. Gerontol. 149 (2021) 101–115, https://doi.org/10.1016/j.exger.2021.111336.
[4] L. Nwidu, E. Elmorsy, J. Aprioku, I. Siminialayi, W. Carter, In vitro anti-cholinesterase and antioxidant activity of extracts of moringa oleifera plants from rivers state, Niger delta, Nigeria, Medicine (Baltim.) 5 (2018) 71, https://doi.org/10.3390/medicines5030071.
[5] D.A. Casey, D. Antimisiaris, J. O'Brien, Drugs for Alzheimer's disease: are they effective? P T 35 (2010) 208–211.
[6] M. Citron, T.S. Diehl, G. Gordon, A.L. Biere, P. Seubert, D.J. Selkoe, Evidence that the 42- and 40-amino acid forms of amyloid β protein are generated from the β-amyloid precursor protein by different protease activities, Proc. Natl. Acad. Sci. U.S.A. 93 (1996) 13170–13175, https://doi.org/10.1073/pnas.93.23.13170.
[7] S. Satarker, P.C. Gurram, A. Nassar, S. Manandhar, R. Vibhavari, D.L. Yarlagadda, J. Mudgal, S. Lewis, D. Arora, M. Nampoothiri, Evaluating the role of N-Acetyl-L-Tryptophan in the Aβ 1-42-induced neuroinflammation and cognitive decline in Alzheimer's disease, Mol. Neurobiol. (2023), https://doi.org/10.1007/s12035-023-03844-4.
[8] M.A. Mengstie, E. Chekol Abebe, A. Behaile Teklemariam, A. Tilahun Mulu, M.M. Agidew, M. Teshome Azezew, E.A. Zewde, A. Agegnehu Teshome, Endogenous advanced glycation end products in the pathogenesis of chronic diabetic complications, Front. Mol. Biosci. 9 (2022) 1–11, https://doi.org/10.3389/fmolb.2022.1002710.
[9] V.N. Bukke, M. Archana, R. Villani, A.D. Romano, A. Wawrzyniak, K. Balawender, S. Orkisz, S. Beggiato, G. Serviddio, T. Cassano, The Dual Role of Glutamatergic Neurotransmission in Alzheimer ' S Disease : from Pathophysiology to Pharmacotherapy, (n.d.) 1–28.
[10] X.Q. Chen, W.C. Mobley, Exploring the pathogenesis of Alzheimer disease in basal forebrain cholinergic neurons:Converging insights from alternative hypotheses, Front. Neurosci. 13 (2019) 1–18, https://doi.org/10.3389/fnins.2019.00446.
[11] C.A. Rankin, Q. Sun, T.C. Gamblin, Tau phosphorylation by GSK-3β promotes tangle-like filament morphology, Mol. Neurodegener. 2 (2007) 1–14.
[12] I.J. Reynolds, T.G. Hastings, Glutamate induces the production of reactive oxygen species in cultured forebrain neurons following NMDA receptor activation, J. Neurosci. 15 (1995) 3318–3327, https://doi.org/10.1523/jneurosci.15-05-03318.1995.
[13] R.T. Bartus, R.L. Dean III, B. Beer, A.S. Lippa, The cholinergic hypothesis of geriatric memory dysfunction, Science 217 (1982) 408–414.
[14] H. Dong, Y. Zhang, Y. Huang, H. Deng, Pathophysiology of RAGE in inflammatory diseases, Front. Immunol. 13 (2022) 1–16, https://doi.org/10.3389/fimmu.2022.931473.
[15] S.A. Beshir, A.M. Aadithsoorya, A. Parveen, S.S.L. Goh, N. Hussain, V.B. Menon, Aducanumab therapy to treat Alzheimer's disease: a narrative review, Int. J. Alzheimer's Dis. 2022 (2022), https://doi.org/10.1155/2022/9343514.
[16] B. Das, R. Yan, A close look at BACE1 inhibitors for Alzheimer's disease treatment, CNS Drugs 33 (2019) 251–263.
[17] S. Lovestone, M. Boada, B. Dubois, M. Hüll, J.O. Rinne, H.-J. Huppertz, M. Calero, M. V Andrés, B. Gómez-Carrillo, T. León, A phase II trial of tideglusib in Alzheimer's disease, J. Alzheim. Dis. 45 (2015) 75–88.
[18] C.-X. Gong, F. Liu, K. Iqbal, Multifactorial hypothesis and multi-targets for Alzheimer's disease, J. Alzheim. Dis. 64 (2018) S107–S117.
[19] G. Brahmachari, D. Gorai, R. Roy, Argemone mexicana: chemical and pharmacological aspects, Rev. Bras. Farmacogn. 23 (2013) 559–575, https://doi.org/10.1590/S0102-695X2013005000021.
[20] J. Jaiswal, N.J. Siddiqi, S. Fatima, M. Abudawood, S.K. AlDaihan, M.G. Alharbi, M. de Lourdes Pereira, P. Sharma, B. Sharma, Analysis of biochemical and antimicrobial properties of bioactive molecules of Argemone mexicana, Molecules 28 (2023), https://doi.org/10.3390/molecules28114428.
[21] N. Singh, B. Sharma, Comparative phytochemical characterization of the Argemone mexicana and Thevetia peruviana leaves extracts, Asian J. Bio. Sci. 13 (2019) 264–269.

[22] J. Jaiswal, B. Sharma, A comparative study of antimicrobial and pharmacological properties of Argemone mexicana, Solanum xanthocarpum and Thevetia peruviana, Acta Sci Microbiol 3 (2020) 1–5.
[23] M.M. Rahman, M.M. Kabir, M.A. AL Noman, M.R. Islam, B.K. Dash, S. Akhter, M.J. Uddin, A. Rahman, Mikania cordata leaves extract promotes activity against pathogenic bacteria and anticancer activity in EAC cell-bearing swiss albino mice, J. Appl. Pharmaceut. Sci. 10 (2020) 112–122, https://doi.org/10.7324/JAPS.2020.102017.
[24] R. Alam, R.R. Imon, M.E. Kabir Talukder, S. Akhter, M.A. Hossain, F. Ahammad, M.M. Rahman, GC-MS analysis of phytoconstituents fromRuellia prostrataandSenna toraand identification of potential anti-viral activity against SARS-CoV-2, RSC Adv. 11 (2021) 40120–40135, https://doi.org/10.1039/d1ra06842c.
[25] J. Cheung, M.J. Rudolph, F. Burshteyn, M.S. Cassidy, E.N. Gary, J. Love, M.C. Franklin, J.J. Height, Structures of human acetylcholinesterase in complex with pharmacologically important ligands, J. Med. Chem. 55 (2012) 10282–10286, https://doi.org/10.1021/jm300871x.
[26] Y. Nicolet, O. Lockridge, P. Masson, J.C. Fontecilla-Camps, F. Nachon, Crystal structure of human butyrylcholinesterase and of its complexes with substrate and products, J. Biol. Chem. 278 (2003) 41141–41147, https://doi.org/10.1074/jbc.M210241200.
[27] K.W. Hunt, A.W. Cook, R.J. Watts, C.T. Clark, G. Vigers, D. Smith, A.T. Metcalf, I.W. Gunawardana, M. Burkard, A.A. Cox, M.K. Geck Do, D. Dutcher, A. A. Thomas, S. Rana, N.C. Kallan, R.K. Delisle, J.P. Rizzi, K. Regal, D. Sammond, R. Groneberg, M. Siu, H. Purkey, J.P. Lyssikatos, A. Marlow, X. Liu, T.P. Tang, Spirocyclic β-site amyloid precursor protein cleaving enzyme 1 (BACE1) inhibitors: from hit to lowering of cerebrospinal fluid (CSF) amyloid β in a higher species, J. Med. Chem. 56 (2013) 3379–3403, https://doi.org/10.1021/jm4002154.
[28] R. Bhat, Y. Xue, S. Berg, S. Hellberg, M. Ormö, Y. Nilsson, A.C. Radesäter, E. Jerning, P.O. Markgren, T. Borgegård, M. Nylöf, A. Giménez-Cassina, F. Hernández, J.J. Lucas, J. Díaz-Nido, J. Avila, Structural insights and biological effects of glycogen synthase kinase 3-specific inhibitor AR-a014418, J. Biol. Chem. 278 (2003) 45937–45945, https://doi.org/10.1074/jbc.M306268200.
[29] G. Madhavi Sastry, M. Adzhigirey, T. Day, R. Annabhimoju, W. Sherman, Protein and ligand preparation: parameters, protocols, and influence on virtual screening enrichments, J. Comput. Aided Mol. Des. 27 (2013) 221–234, https://doi.org/10.1007/s10822-013-9644-8.
[30] S. Akhter, M.W. Hossain, S. Sultana, J. Ferdous Jharna, N. Sultana Meghla, R. Alam, K.M. Anis-Ul-Haque, M. Mashiar Rahman, Ruellia prostrata Poir. activity evaluated by phytoconstituents, antioxidant, anti-inflammatory, antibacterial activity, and in silico molecular functions, J. Saudi Chem. Soc. 26 (2022) 101401, https://doi.org/10.1016/j.jscs.2021.101401.
[31] M.M. Rahman, M.A. Al Noman, S. Khatun, R. Alam, M.M.H. Shetu, E.K. Talukder, R.R. Imon, M.Y. Biswas, K.M. Anis-Ul-Haque, M.J. Uddin, S. Akhter, Evaluation of Senna tora (L.) Roxb. leaves as source of bioactive molecules with antioxidant, anti-inflammatory and antibacterial potential, Heliyon 9 (2023) e12855, https://doi.org/10.1016/j.heliyon.2023.e12855.
[32] S. Rakesh, A.K. Pandey, A. Roy, Assessment of secondary metabolites, in-vitro antioxidant and anti-inflammatory activity of root of Argemone mexicana L, ES Food Agrofor (2023) 1–12, https://doi.org/10.30919/esfaf1007.
[33] A.I. Arcos-Martínez, O.D. Muñoz-Muñiz, M.Á. Domínguez-Ortiz, M.V. Saavedra-Vélez, M. Vázquez-Hernández, M.G. Alcántara-López, Anxiolytic-like effect of ethanolic extract of Argemone mexicana and its alkaloids in Wistar rats, Avicenna J. Phytomedicine 6 (2016) 476–488, ncbi.nlm.nih.gov/pubmed/27516989%0Ahttp://www.pubmedcentral.nih.gov/articlerender.fcgi?artid=PMC4967844.
[34] J. Mahendra, Study of Anti-diabetic Activities and Secondary Metabolite Production in Nyctanthes Arbor-Tristis, vol. 12, 2023, pp. 8011–8016. https://www.researchgate.net/publication/373247106.
[35] W.P. Walters, M.T. Stahl, M.A. Murcko, Virtual screening—an overview, Drug Discov. Today 3 (1998) 160–178.
[36] N.J. Joshi, A.R.S. Reddy, Navigating the GSK-3β inhibitors as versatile multi-target drug ligands in Alzheimer's disease intervention–A comprehensive review, Results Chem (2024) 101500.
[37] A. Samad, M.A. Huq, M.S. Rahman, Bioinformatics approaches identified dasatinib and bortezomib inhibit the activity of MCM7 protein as a potential treatment against human cancer, Sci. Rep. 12 (2022) 1–16, https://doi.org/10.1038/s41598-022-05621-0.
[38] Z. Cai, C. Wang, W. Yang, Role of berberine in Alzheimer's disease, Neuropsychiatric Dis. Treat. 12 (2016) 2509–2520, https://doi.org/10.2147/NDT.S114846.
[39] H. Zhang, C. Zhao, G. Cao, L. Guo, S. Zhang, Y. Liang, C. Qin, P. Su, H. Li, W. Zhang, Berberine modulates amyloid-β peptide generation by activating AMP-activated protein kinase, Neuropharmacology 125 (2017) 408–417, https://doi.org/10.1016/j.neuropharm.2017.08.013.
[40] E.V. Leitao da-Cunha, I.M. Fechine, D.N. Guedes, J.M. Barbosa-Filho, M. Sobral da Silva, Protoberberine alkaloids, alkaloids, Chem. Biol. 62 (2005) 1–75, https://doi.org/10.1016/S1099-4831(05)62001-9.
[41] Z. Dong, S.S. Tang, X.L. Ma, B. Tan, Z.S. Tang, C.H. Li, Z.H. Yang, J.G. Zeng, Acute, chronic, and genotoxic studies on the protopine total alkaloids of the Macleaya cordata (willd.) R. Br. in rodents, Front. Pharmacol. 13 (2022), https://doi.org/10.3389/fphar.2022.987800.
[42] C. Nie, B. Wang, B. Wang, N. Lv, R. Yu, E. Zhang, Protopine triggers apoptosis via the intrinsic pathway and regulation of ROS/PI3K/Akt signalling pathway in liver carcinoma, Cancer Cell Int. 21 (2021) 1–10, https://doi.org/10.1186/s12935-021-02105-5.
[43] X. Xiao, J. Liu, J. Hu, T. Li, Y. Zhang, Protective effect of protopine on the focal cerebral ischaemic injury in rats, Basic Clin. Pharmacol. Toxicol. 101 (2007) 85–89, https://doi.org/10.1111/j.1742-7843.2007.00075.x.
[44] E. Plazas, M.C. Avila M, D.R. Muñoz, L.E. Cuca S, Natural isoquinoline alkaloids: pharmacological features and multi-target potential for complex diseases, Pharmacol. Res. 177 (2022), https://doi.org/10.1016/j.phrs.2022.106126.
[45] Y. Prokopenko, V. Tsyvunin, S. Shtrygol, V. Georgiyants, In vivo anticonvulsant activity of extracts and protopine from the Fumaria schleicheri herb, Sci. Pharm. 84 (2016) 547–554, https://doi.org/10.3390/scipharm84030547.
[46] L.F. Xu, W.J. Chu, X.Y. Qing, S. Li, X.S. Wang, G.W. Qing, J. Fei, L.H. Guo, Protopine inhibits serotonin transporter and noradrenaline transporter and has the antidepressant-like effect in mice models, Neuropharmacology 50 (2006) 934–940, https://doi.org/10.1016/j.neuropharm.2006.01.003.
[47] P. Devi, A.N. Syad, Botanics: a potential source of new therapies for Alzheimer's disease? Botanics Targets Ther. (2014) 11, https://doi.org/10.2147/btat.s33554.
[48] A. Edinoff, N. Sathivadivel, T. McBride, A. Parker, C. Okeagu, A.D. Kaye, A.M. Kaye, J.S. Kaye, R.J. Kaye, M.M. Sheth, O. Viswanath, I. Urits, Chronic pain treatment strategies in Parkinson's disease, Neurol, Int. 12 (2020) 61–76, https://doi.org/10.3390/neurolint12030014.
[49] M.C. Van Hout, E. Rich, S. Dada, M. Bergin, "codeine is my helper": misuse of and dependence on codeine-containing medicines in South Africa, Qual. Health Res. 27 (2017) 341–350, https://doi.org/10.1177/1049732315613764.
[50] C. Morén, R.M. deSouza, D.M. Giraldo, C. Uff, Antioxidant therapeutic strategies in neurodegenerative diseases, Int. J. Mol. Sci. 23 (2022), https://doi.org/10.3390/ijms23169328.